J. Fluid Mech. (1996), *vol.* 329, *pp.* 207–245

Nonlinear deformation and breakup of stretching liquid bridges

By X. ZHANG[1], R. S. PADGETT[2] AND O. A. BASARAN[3]

[1]Chemical Technology Division, Oak Ridge National Laboratory, Oak Ridge, TN 37831-6224, USA

[2]Department of Chemical Engineering, University of Tennessee, Knoxville, TN 37996, USA

[3]School of Chemical Engineering, Purdue University, W. Lafayette, IN 47907-1283, USA

(Received 22 December 1995 and in revised form 23 June 1996)

In this paper, the nonlinear dynamics of an axisymmetric liquid bridge held captive between two coaxial, circular, solid disks that are separated at a constant velocity are considered. As the disks are continuously pulled apart, the bridge deforms and ultimately breaks when its length attains a limiting value, producing two drops that are supported on the two disks. The evolution in time of the bridge shape and the rupture of the interface are investigated theoretically and experimentally to quantitatively probe the influence of physical and geometrical parameters on the dynamics. In the computations, a one-dimensional model that is based on the slender jet approximation is used to simulate the dynamic response of the bridge to the continuous uniaxial stretching. The governing system of nonlinear, time-dependent equations is solved numerically by a method of lines that uses the Galerkin/finite element method for discretization in space and an adaptive, implicit finite difference technique for discretization in time. In order to verify the model and computational results, extensive experiments are performed by using an ultra-high-speed video system to monitor the dynamics of liquid bridges with a time resolution of 1/12th of a millisecond. The computational and experimental results show that as the importance of the inertial force – most easily changed in experiments by changing the stretching velocity – relative to the surface tension force increases but does not become too large and the importance of the viscous force – most easily changed by changing liquid viscosity – relative to the surface tension force increases, the limiting length that a liquid bridge is able to attain before breaking increases. By contrast, increasing the gravitational force – most readily controlled by varying disk radius or liquid density – relative to the surface tension force reduces the limiting bridge length at breakup. Moreover, the manner in which the bridge volume is partitioned between the pendant and sessile drops that result upon breakup is strongly influenced by the magnitudes of viscous, inertial, and gravitational forces relative to surface tension ones. Attention is also paid here to the dynamics of the liquid thread that connects the two portions of the bridge liquid that are pendant from the top moving rod and sessile on the lower stationary rod because the manner in which the thread evolves in time and breaks has important implications for the closely related problem of drop formation from a capillary. Reassuringly, the computations and the experimental measurements are shown to agree well with one another.

1. Introduction

Plateau (1863) and Rayleigh (1879) have shown theoretically that although an infinitely long, cylindrical column of fluid is an equilibrium shape in zero gravity, it is unstable to all infinitesimal-amplitude, axisymmetric perturbations whose wavelengths exceed the circumference of the cylinder (see, also, Michael 1981). Moreover, Plateau was able to show experimentally that a cylindrical column of fluid that is neutrally buoyant in the surrounding ambient fluid can be held in stable equilibrium between two coaxial solid disks of equal radii as a *liquid bridge* provided that the ratio of the length of the bridge to its diameter is less than a critical value. This critical value has been shown to lie between 3.13 and 3.18 by Plateau in his pioneering experiments and between 3.140 and 3.1417 by Mason (1970) through more refined experiments.

When a static liquid bridge that is in stable equilibrium for times less than zero is impulsively set in motion at time zero and stretched uniaxially for times exceeding zero by continuously pulling apart the two disks at a constant velocity, it deforms gradually and contracts at its middle portion. Figure 1 illustrates the evolution in time of the shape of an axisymmetric water bridge that is surrounded by air and whose axis of symmetry lies along the direction of gravity (which acts downward in the photographs). The time sequence of photographs shows the transient shape of a bridge that is stretched by moving the top disk at a constant velocity of 0.6 cm s^{-1} relative to the bottom disk which is stationary. Of great interest in the dynamics depicted in figure 1 is the fate of a thin liquid thread that as time advances develops and connects the two large liquid masses which are supported on the two disks during the necking and breakup of the bridge. During necking, the portion of the bridge below the thread tends to take on a spherical profile and that above the thread approximates well a liquid cone. Meanwhile, the length of the thread increases while its diameter decreases, as shown in figure 1(*h–j*). When the length of the liquid bridge attains a limiting value, the thread ruptures (figure 1*j*) and subsequently two large drops whose volumes may nevertheless be unequal are created such that one is pendant from the top disk and the other is sessile on the bottom disk. Furthermore, following the rupture of the liquid thread one or more satellite droplets may be generated and occupy the region between the pendant and sessile drops in some situations (not shown in figure 1). The satellite droplets, if they exist, are much smaller in size, or volume, than the supported drops. In this paper, a theoretical/experimental study is presented of the dynamics of uniaxially stretched liquid bridges in air. The focus here is on the effects of physical and geometrical parameters on the universal features of bridge deformation. Special attention is also paid to the development, extension and breakup of the liquid thread *and* the generation of pendant and sessile drops that are created subsequent to the breakup of the liquid bridge.

The statics and dynamics of liquid bridges have attracted much attention for more than a century. However, interest in their response has been growing in recent years due to applications in fields as diverse as (i) the floating-zone technique for crystal growth where they provide useful idealizations (Brown 1988), (ii) controlling of thermocapillary convection in a liquid bridge, which is readily achieved by vibrating one of the supporting rods (Anilkumar *et al.* 1993), (iii) the spraying and atomization of liquids where a fundamental understanding of the breakup of liquid columns is essential (Schulkes 1993*a*; see, also, Schulkes 1993*b* and Papageorgiou 1995*a,b*), (iv) the fibre spinning process (Denn 1980), (v) the measurement of the surface tension, shear viscosity, and extensional viscosity of molten Newtonian and non-Newtonian liquids (Tsamopoulos, Chen & Borkar 1992; Tirtaatmadja & Sridhar 1993), and (vi)

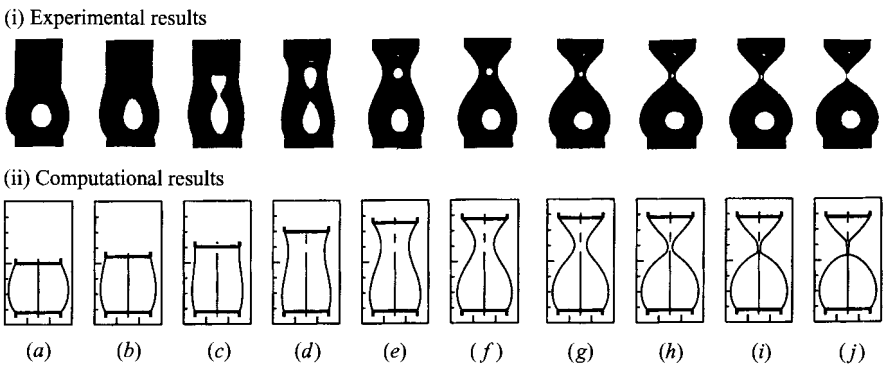

FIGURE 1. Evolution in time of the experimentally measured and computed shape of a water bridge of volume of 0.04 cm^3 and initial slenderness ratio of 2 that is held captive between two circular rods of equal radii of 0.16 cm and is stretched axially at a constant velocity of 0.6 cm s^{-1}: (*a*) $t = 0$ ms, (*b*) $t = 67$ ms, (*c*) $t = 175$ ms, (*d*) $t = 333$ ms, (*e*) $t = 427$ ms, (*f*) $t = 462$ ms, (*g*) $t = 469$ ms, (*h*) $t = 471$ ms, (*i*) $t = 471.5$ ms, and (*j*) $t = 472$ ms, where t is the time measured from the instant when the upper rod is set into motion.

agglomeration of particles (Ennis *et al.* 1990; Chen, Tsamopoulos & Good 1992). Of special interest to the present authors and yet another motivation is the close analogy between interface rupture during drop formation from a capillary (Zhang & Basaran 1995, 1996) and liquid bridge breakup.

Until about 1980, virtually all experimental and theoretical studies of liquid bridges were focused on the equilibrium shapes of bridges and their stability. Most of these works have addressed the situation in which an axisymmetric liquid bridge is held captive between two axially aligned circular disks of equal radii in the absence and presence of gravity (Haynes 1970; Gillette & Dyson 1971; Coriell, Hardy & Cordes 1977; and Russo & Steen 1986, among others). Especially noteworthy among these is the work of Coriell *et al.* (1977) where it is shown that the maximum stable length of the bridge decreases significantly as the gravitational force increases. Studies of fully three-dimensional shapes of liquid bridges are scarcer but profiles of such menisci have been calculated by Patzek & Scriven (1982) for drops held captive between two crossed cylinders, Chen *et al.* (1992) for bridges held captive between non-parallel surfaces, and Brown & Scriven (1980) and Ungar & Brown (1982) for liquid bridges undergoing gyrostatic rotation.

Although Mason (1970) demonstrated that it is possible to establish standing waves on the surface of a liquid bridge by oscillating the supporting disks or rods, it was not until after the work of Fowle, Wang & Strong (1979) that the dynamics and breakup of liquid bridges began to be studied extensively due to motivation provided by the European and American Space Programs. Fowle *et al.* (1979) carried out experiments similar to those performed by Mason (1970) and also carried out a linearized analysis of the oscillations of a bridge of an inviscid liquid undergoing irrotational flow. Much of the subsequent theoretical work on the dynamics of liquid bridges has either relied on one-dimensional models or taken the bridge liquid, and the fluid surrounding it, to be inviscid. The one-dimensional models have been developed under the assumption that the bridge is sufficiently slender so that the axial velocity is independent of the radial coordinate and depends solely on the axial coordinate and time. However, two fundamentally different one-dimensional models have been used to analyse the dy-

namics of liquid bridges. The first one is the inviscid slice model due to Lee (1974) and the second one is the model based on the so-called Cosserat equations (Green 1976).

Meseguer (1983) studied theoretically by means of both the inviscid slice model and the Cosserat equations the breakup of axisymmetric liquid bridges of initial slenderness ratios, i.e. the ratio of the bridge length to the rod radius, close to those at their limits of static stability by subjecting them to axisymmetric disturbances. Meseguer & Sanz (1985) studied theoretically using the one-dimensional inviscid slice model the axisymmetric breakup of bridges under microgravity conditions and carried out experiments with nearly neutrally buoyant liquid bridges. Sanz (1985) studied both theoretically and experimentally the effect of an outer bath on the dynamics of axisymmetric liquid bridges. He studied the breakup of the liquid bridge theoretically by means of the one-dimensional inviscid slice model. Moreover, he constructed a linearized but inviscid model and carried out experiments to study the oscillations of the liquid bridge. Non-axisymmetric oscillations were later studied by Sanz & Diez (1989) who developed a linearized, inviscid theory and carried out experiments. Bridge oscillations due to variations in the level of microgravity are also of interest and have been studied by means of one-dimensional models. Zhang & Alexander (1990) used a one-dimensional model with viscosity to determine the response of liquid bridges subjected to harmonic disturbances. Meseguer & Perales (1991) used the one-dimensional Cosserat equations with viscosity and determined the response of liquid bridges to small but step changes in the level of microgravity. Much of the work in this area has been reviewed by Perales & Meseguer (1992) who have also studied experimentally and theoretically by means of the one-dimensional Cosserat equations with viscosity the oscillations of liquid bridges induced by vibrating the supporting rods.

Because the assumption of restricting the bridge to be an inviscid liquid is severely restricting, Tsamopoulos and coworkers carried out several studies to elucidate the effect of finite viscosity on the dynamics of liquid bridges. Borkar & Tsamopoulos (1991) carried out a boundary layer analysis to account for the effect of small viscosity and studied the infinitesimal-amplitude oscillations of axisymmetric, capillary bridges in the limit of large but not infinite Reynolds number. Tsamopoulos *et al.* (1992) studied the small-amplitude oscillations of liquid bridges of arbitrary viscosity. However, in contrast to the case of oscillations of free drops (cf. Miller & Scriven 1968), the presence of solid boundaries gives rise to an implicit eigenvalue problem such that the determination of each eigenmode of oscillation involves an infinite summation (cf. the case of oscillating pendant drops studied by Strani & Sabetta 1988). Therefore, Tsamopoulos *et al.* (1992) used the finite element method to reduce the linearized perturbation equations to an algebraic generalized eigenvalue problem, which they then solved to obtain the linearized eigenfrequencies of oscillation and damping rates. Subsequently, Chen & Tsamopoulos (1993) used the Galerkin/finite element method and Mollot *et al.* (1993) carried out experiments to study the finite-amplitude, forced oscillations of liquid bridges induced by vibrating the top rod while holding the bottom rod fixed. Through their fundamental studies, Tsamopoulos *et al.* (1992) and Chen & Tsamopoulos (1993) showed that the resonant frequency of oscillation decreases and the damping rate increases linearly with the oscillation amplitude. These authors then demonstrated that careful measurement of these two quantities, coupled to the computations, can be used to provide accurate values of physical properties such as viscosity and surface tension of the bridge liquid, in particular for high-temperature molten ceramics and semiconductors.

By contrast to the problem of an oscillating liquid bridge, the problem of a stretching liquid bridge has received relatively little attention to date. Moreover, virtually all of the previous theoretical and experimental work on stretching liquid bridges has been motivated by and aimed at characterizing the rheological response of polymeric liquids to uniaxial extension. Motivated by the desire to simulate the extensional rheometry experiments of Sridhar *et al.* (1991), Shipman, Denn & Keunings (1991) used the finite element method to solve the free boundary problem that describes the stretching of a viscoelastic liquid bridge. Although this was a pioneering computational study, these authors experienced numerical difficulties because their code required that the length of the computational domain be fixed in the axial direction, i.e. the direction in which the bridge is being elongated. Kroger *et al.* (1992) examined the deformation of liquid bridges of large volumes in a series of simple stretching experiments in a Plateau tank in order to understand the influence of various forces (i.e. interfacial tension, inertial, and viscous forces) on the deformation and breakup of liquid bridges. Based on the stretching behaviour of bridges of various Newtonian liquids, Kroger *et al.* (1992) observed that while the interfacial tension force contracts and, eventually, breaks a stretching liquid bridge, inertial and viscous forces tend to stabilize the bridge surface and significantly slow down its breakup. These authors found that at large disk velocities, the bridge shapes do not attain equilibrium profiles appropriate for the instantaneous value of the slenderness ratio and the limiting length of the bridge exceeds the critical length of a static bridge at its limit of stability. These authors further found that the effects of inertia on the dynamics of a stretching bridge cannot be neglected even at elongation rates as low as 0.1 s^{-1}. Moreover, it is noteworthy that the minimum value of the bridge radius reported in these experiments was about 4% of the initial radius, which indicates a lack of understanding of the final stages of the breakup. Kroger & Rath (1995) carried out a set of beautiful visualization experiments in which they utilized a sheet of light to illuminate the motion of a set of tracer particles inside stretching liquid bridges. These authors then determined the local rates of elongation and shear rate distributions inside the bridges from the pathlines of the tracer particles. Gaudet, McKinley & Stone (1994) used the boundary integral method to determine the transient deformation of Newtonian liquid bridges without breakup in the limit of Stokes flow as a preliminary to the design and interpretation of experiments for measuring extensional viscosity of non-Newtonian fluids.

Hence, although qualitative features of the dynamics of stretching liquid bridges are known through the previously cited studies, a quantitative understanding of the effects of geometric variables and physical properties that govern the nonlinear deformation and breakup of stretching liquid bridges has heretofore been lacking. These insights are gained in this work by a dual-pronged approach that places equal emphasis on computation and experiment. In the computations, a system of equations based on a one-dimensional model of the stretching liquid bridge is solved by the Galerkin/finite element method. The one-dimensional equations are those that result from the transient Navier–Stokes equation and accompanying interfacial boundary conditions by either (i) retaining the leading-order terms in a Taylor series expansion in the radial coordinate of the velocity and pressure fields and free-surface location (Eggers & Dupont 1994) or (ii) carrying out an asymptotic expansion under a slender-jet or long-wave approximation to capture the leading-order dynamics (Papageorgiou 1995*a*). The experiments rely on an ultra-high-speed motion analysis and video system that can monitor instantaneous shapes of stretching liquid bridges with a time resolution down to 1/12th of a millisecond. Section 2 presents the one-dimensional equations,

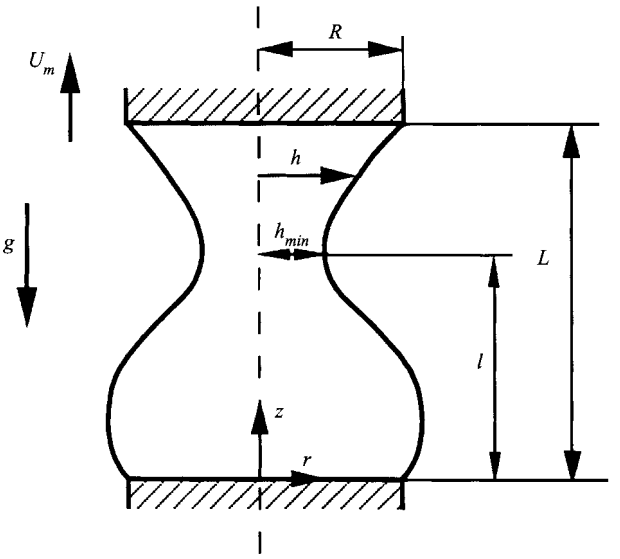

FIGURE 2. Schematic of a liquid bridge held captive between two rods under gravity that highlights certain dimensions that are useful in describing bridge deformation and breakup.

boundary conditions, and initial conditions that govern the dynamics. The numerical method used to solve the set of evolution equations and associated boundary and initial conditions is described in §3. Section 4 describes the experimental apparatus, materials, and methods of data acquisition and analysis. Section 5 presents results of detailed computations and compares the numerical predictions to experimental measurements. In both §5 and §6, concluding remarks, analogies are drawn between the present problem and the closely related one of drop formation from capillaries.

2. Problem formulation

The system is an axisymmetric bridge of fixed volume V of an incompressible, Newtonian liquid of spatially uniform and constant viscosity μ and density ρ. As shown in figure 2, the bridge is captured between and is coaxial with two solid circular disks or rods of equal radii R that are separated by an initial distance L_0 from each other. The common axis of symmetry of the bridge and the disks is vertical and lies along the direction of the gravity vector $\boldsymbol{g}$. The liquid wets completely the two planar surfaces of the disks: the two contact lines are circles that are pinned to the edges of the disks, irrespective of the state of motions of the bridge and the disks. Here the top disk is taken to move upward along the axis of symmetry at a constant velocity U_m while the bottom disk is taken to be stationary. The ambient fluid – here air – exerts uniform pressure and negligible viscous drag on the bridge. The surface tension σ of the liquid–gas interface is also spatially uniform and constant in time. In what follows, it is convenient to define a cylindrical coordinate system $\{r, z, \phi\}$, whose origin lies at the centre of the lower disk surface, and where r denotes the radial coordinate, z the axial coordinate measured in the direction opposite to gravity, and ϕ the azimuthal angle. For the axisymmetric configurations of interest in this paper, the problem is independent of the azimuthal coordinate.

Isothermal, transient flow of a viscous liquid inside a stretching bridge is governed by the Navier–Stokes system and appropriate boundary and initial conditions. Follow-

ing Eggers & Dupont (1994) and Papageorgiou (1995*a*), this spatially two-dimensional system of partial differential equations is reduced to a spatially one-dimensional system as discussed in the Introduction. The equations that govern the axial velocity $v \equiv v(z,t)$ and the bridge profile $h \equiv h(z,t)$, where t is time, are

$$\frac{\partial \tilde{v}}{\partial \tilde{t}} = -\tilde{v}\frac{\partial \tilde{v}}{\partial \tilde{z}} - Oh\frac{\partial \tilde{p}}{\partial \tilde{z}} + 3\,Oh\frac{1}{\tilde{h}^2}\frac{\partial}{\partial \tilde{z}}\left(\tilde{h}^2\frac{\partial \tilde{v}}{\partial \tilde{z}}\right) - G, \tag{1}$$

$$\frac{\partial \tilde{h}}{\partial \tilde{t}} = -\tilde{v}\frac{\partial \tilde{h}}{\partial \tilde{z}} - \frac{1}{2}\frac{\partial \tilde{v}}{\partial \tilde{z}}\tilde{h}. \tag{2}$$

Equations (1) and (2) are already dimensionless because length is measured in units of R and time in units of $\tau \equiv (\rho R^3/\sigma)^{1/2}$. With these choices for the length and time scales, the velocity scale is not independent but is given by $U \equiv R/\tau = (\sigma/\rho R)^{1/2}$. In equations (1) and (2) and throughout the remainder of this paper, variables that appear with a tilde over them are dimensionless counterparts of those without tildes. In equation (1), $Oh \equiv \mu/(\rho R\sigma)^{1/2}$ is the Ohnesorge number, which measures the importance of viscous forces relative to surface tension forces and $G \equiv \rho R^2 g/\sigma$, where g is the magnitude of the acceleration due to gravity, is the gravitational Bond number, which measures the importance of gravitational forces relative to surface tension forces. Moreover, the modified dimensionless pressure $\tilde{p}$, which is measured in units of σ/R and whose axial derivative appears in equation (1), is related to twice the dimensionless local mean curvature of the interface by

$$Oh\,\tilde{p} = \frac{1}{\tilde{h}[1+(\partial \tilde{h}/\partial \tilde{z})^2]^{1/2}} - \frac{\partial^2 \tilde{h}/\partial \tilde{z}^2}{[1+(\partial \tilde{h}/\partial \tilde{z})^2]^{3/2}}. \tag{3}$$

The dimensionless pressure $\tilde{\mathscr{P}}$ inside the liquid bridge to leading order is then given by (cf. Eggers & Dupont 1994)

$$\tilde{\mathscr{P}} = Oh\left(\tilde{p} - \frac{\partial \tilde{v}}{\partial \tilde{z}}\right). \tag{4}$$

As shown by Papageorgiou (1995*a*), keeping the full curvature term, equation (3), in the asymptotically correct slender bridge equation (1) is not rational. However, Eggers & Dupont (1994) who studied drop formation and Ruschak (1978), Kheshgi (1989), and Johnson *et al.* (1991) who studied the dynamics of thin films over flat and cylindrical substrates have also adopted this approach because doing so results in a better description of the nonlinear evolution of interface shapes than truncating the curvature expression at the order demanded by the leading-order slender jet asymptotics. Moreover, we go beyond these previous works in which the full expression for twice the local mean curvature is utilized and carry out a complementary program of laboratory observation to evaluate the validity of this approximation.

Equations (1)–(3) are solved subject to the boundary conditions that the three-phase contact lines, where the bridge liquid, the ambient fluid, and the solid surfaces meet, remain pinned for all time $\tilde{t} > 0$:

$$\tilde{h}(\tilde{z}=0,\tilde{t}) = 1, \quad \tilde{h}(\tilde{z}=L/R,\tilde{t}) = 1 \tag{5a,b}$$

and the axial velocity vanishes at the bottom disk surface and equals the disk velocity at the top disk surface:

$$\tilde{v}(\tilde{z}=0,\tilde{t}) = 0, \quad \tilde{v}(\tilde{z}=L/R,\tilde{t}) = \tilde{U}_m. \tag{6a,b}$$

In equations (5) and (6) L is the dimensional instantaneous length of the liquid bridge and in equation (6*b*) the dimensionless disk velocity $\tilde{U}_m \equiv U_m/U = U_m(\rho R/\sigma)^{1/2}$ measures the importance of inertial forces relative to surface tension forces.

We seek solutions of the nonlinear, time-dependent partial differential equations (1)–(2) subject to boundary conditions (5)–(6). Initial conditions must be specified to complete the mathematical statement of the problem. In this paper, attention is restricted to situations in which the bridge is impulsively set into motion from an initial rest state that corresponds to a stable equilibrium shape of a captive bridge of volume V/R^3, initial slenderness ratio L_0/R, and under the condition that the gravitational Bond number equals some specified value G, namely

$$\tilde{h}(\tilde{z}, \tilde{t} = 0) = \tilde{h}_0(\tilde{z}), \tag{7}$$

$$\tilde{v}(\tilde{z}, \tilde{t} = 0) = 0, \tag{8}$$

where $\tilde{h}_0$ is the interface shape function of the equilibrium shape. The equilibrium bridge shape is governed the Young–Laplace equation (see e.g. Brown & Scriven 1980)

$$-2\tilde{\mathscr{H}} = K - G\tilde{z}, \tag{9}$$

where $2\tilde{\mathscr{H}}$ is twice the dimensionless local mean curvature of the interface given by equation (3) and K is the reference pressure. When the volume of the bridge is fixed to be a certain amount, the interface shape function $\tilde{h}_0(\tilde{z})$ and the reference pressure K are determined by solving simultaneously the Young–Laplace equation (9) and a constraint of fixed bridge volume

$$\pi \int_0^{L_0/R} \tilde{h}_0^2 \mathrm{d}\tilde{z} = \frac{V}{R^3}. \tag{10}$$

Therefore, whereas the axisymmetric equilibrium shape of a liquid bridge is governed by three parameters, the gravitational Bond number G, the dimensionless volume V/R^3, and the slenderness ratio L_0/R, the dynamics of stretching and breaking bridges are governed by five parameters, namely by the Ohnesorge number Oh and the dimensionless disk velocity $\tilde{U}_m$ in addition to the three parameters that govern the behaviour of static bridges.

The dimensionless variables used in this paper are of course not unique. One could alternatively use the disk velocity U_m as the velocity scale in non-dimensionalizing the governing equations and boundary and initial conditions. In this formulation, Oh and $\tilde{U}_m$ are replaced by a Reynolds number, $Re \equiv \rho R U_m/\mu$, and a capillary number, $Ca \equiv \mu U_m/\sigma$.

In §5, two dimensional measures of bridge deformation are convenient for describing the evolution in time of the shape of the stretching bridge. As shown in figure 2, these are the instantaneous length of the bridge measured along its axis, L, and the instantaneous radius of the bridge neck at the location where it is narrowest, h_{min}. Separated by this minimum radius, a bridge liquid can be divided into two portions that are supported on the two disks during its necking and breakup. When G is non-zero, the shape of the bridge is no longer symmetric about the axial location at which its radius is a minimum and the portion of the bridge attached to the lower disk is of larger volume than that attached to the upper disk. In §5, the volumes of the two supported drops that are generated subsequent to the breakup of the bridge are also monitored for further characterizing the dynamics. Moreover, throughout the remainder of the paper, L_d denotes the limiting length or the maximum length

attained by the bridge at the instant when it breaks and t refers to time measured from the instant at which the stretching of the bridge commences.

3. Finite element analysis

The governing set of one-dimensional, nonlinear equations (1)–(2) is solved numerically in this work by the Galerkin/finite element method (Strang & Fix 1973; Lapidus & Pinder 1982). In this paper, the mathematical problem is reformulated by introducing a new variable Ω so that the highest-order derivative appearing in the governing equations is of second order. This reformulation requires that equations (1)–(2) be augmented by the equation

$$\Omega - \frac{\partial \tilde{h}}{\partial \tilde{z}} = 0. \tag{11}$$

With this reformulation, it is only required that the basis functions that represent the unknowns $\tilde{h}$, Ω, and $\tilde{v}$ be continuous or that they fall into a class of interpolating functions known as C^0 basis functions (Strang & Fix 1973). The domain $0 \leqslant \tilde{z} \leqslant L/R$ is divided into NE elements. The unknowns are then expanded in terms of a series of linear basis functions $\phi^i(\tilde{z})$:

$$\tilde{h}(\tilde{z},\tilde{t}) = \sum_{i=1}^{N} h_i(\tilde{t})\phi^i(\tilde{z}), \tag{12}$$

$$\Omega(\tilde{z},\tilde{t}) = \sum_{i=1}^{N} \Omega_i(\tilde{t})\phi^i(\tilde{z}), \tag{13}$$

$$\tilde{v}(\tilde{z},\tilde{t}) = \sum_{i=1}^{N} v_i(\tilde{t})\phi^i(\tilde{z}), \tag{14}$$

where h_i, Ω_i, and v_i are unknown coefficients to be determined and $N \equiv NE + 1$.

The Galerkin weighted residuals of equations (1), (2), and (11) are constructed by weighting each equation by the basis functions and integrating the resulting expressions over the computational domain. The weighted residuals of equation (1) are next integrated by parts to reduce the order of the highest-order derivative appearing in them and the resulting expressions are then simplified because of boundary conditions (5)–(6). The residual equations are then cast into a fixed isoparametric coordinate system $0 \leqslant \xi \leqslant 1$ by the isoparametric mapping $\tilde{z} = \sum_{i=1}^{N} z_i\phi_i(\xi)$ (Strang & Fix 1973), where the z_i denote the locations of the nodes or the mesh points. Because the top boundary is moving, the domain length changes as time advances. This is accounted for in this paper by allowing the nodes of the finite element mesh z_i to move proportionally to the motion of the top rod (Kistler & Scriven 1983; Kheshgi & Scriven 1983; see, also, Basaran 1992):

$$z_i(\tilde{t}) = z_i(\tilde{t}=0)\frac{L}{L_0}, \quad i = 1,\ldots,N. \tag{15}$$

The evaluation of the residuals then requires that time derivatives at fixed locations in physical space be cast into time derivatives at fixed isoparametric locations by

$$\frac{\mathrm{d}}{\mathrm{d}\tilde{t}} = \frac{\partial}{\partial \tilde{t}} + v_m\frac{\partial}{\partial \tilde{z}}, \tag{16}$$

where $v_m(\tilde{z},\tilde{t}) = \tilde{U}_m\tilde{z}/(L/R)$. With these manipulations, the residual equations become

$$R_M^i = \int_0^1 \left\{ \left[\frac{\mathrm{d}\tilde{v}}{\mathrm{d}\tilde{t}} + (\tilde{v} - v_m)\frac{\partial \tilde{v}}{\partial \tilde{z}} \right] \phi^i - \left[\frac{1}{\tilde{h}(1+\Omega^2)^{1/2}} - \frac{\partial\Omega/\partial\tilde{z}}{(1+\Omega^2)^{3/2}} \right] \frac{\mathrm{d}\phi^i}{\mathrm{d}\tilde{z}} \right.$$
$$\left. -3\,Oh \left(\frac{2}{\tilde{h}}\frac{\partial\tilde{v}}{\partial\tilde{z}}\frac{\partial\tilde{h}}{\partial\tilde{z}}\phi^i - \frac{\partial\tilde{v}}{\partial\tilde{z}}\frac{\mathrm{d}\phi^i}{\mathrm{d}\tilde{z}} \right) + G\phi^i \right\} \tilde{z}_\xi \mathrm{d}\xi, \tag{17}$$

$$R_\Omega^i = \int_0^1 \left(\Omega - \frac{\partial\tilde{h}}{\partial\tilde{z}} \right) \phi^i \tilde{z}_\xi \mathrm{d}\xi, \tag{18}$$

and

$$R_K^i = \int_0^1 \left[\frac{\mathrm{d}\tilde{h}}{\mathrm{d}\tilde{t}} + (\tilde{v} - v_m)\frac{\partial\tilde{h}}{\partial\tilde{z}} + \frac{1}{2}\tilde{h}\frac{\partial\tilde{v}}{\partial\tilde{z}} \right] \phi^i \, \tilde{z}_\xi \mathrm{d}\xi, \tag{19}$$

where $\tilde{z}_\xi \equiv \mathrm{d}\tilde{z}/\mathrm{d}\xi$ and $i = 1,\ldots,N$.

The Galerkin weighted residuals (17)–(19) are a set of nonlinear ordinary differential equations in time. In this paper, time derivatives are discretized at the pth time step, $\Delta\tilde{t}_p = \tilde{t}_p - \tilde{t}_{p-1}$, by either first-order backward differences or second-order trapezoid rule. With time discretization in place, the resulting system of $3N$ nonlinear algebraic equations is solved by Newton's method. Four backward-difference time steps with fixed $\Delta\tilde{t}_p$ provide the necessary smoothing (Luskin & Rannacher 1982) before the trapezoid rule is used. Moreover, in this paper a first-order forward-difference predictor is used with the backward-difference method and a second-order Adams–Bashforth predictor is used with the trapezoid rule. The norm of the correction provided by Newton iterations, $\| d_{p+1} \|_\infty$, is an estimate of the local time truncation error of the trapezoid rule (Gresho, Lee & Sani 1979). The time step is chosen adaptively by requiring the norm of the time truncation error at the next time step to be equal to a prescribed value, ϵ, $\Delta t_{p+1} = \Delta t_p \left(\epsilon / \| d_{p+1} \|_\infty\right)^{1/3}$. Relative error of 0.1% per time step, $\epsilon = 10^{-3}$, is prescribed in the computations.

As summarized in the previous section, the equilibrium shape of a static bridge is required as an initial condition on the interface shape function in the dynamic calculations. The equilibrium shape of a bridge of slenderness ratio L_0/R and volume V/R^3 is determined at a specified value of the gravitational Bond number G by Galerkin/finite element analysis (see, e.g., Brown & Scriven 1980). Both the algorithm for calculating static shapes and that for computing the transient evolution of shapes of stretching bridges have been programmed in FORTRAN and the resulting codes have been run on a Silicon Graphics Indigo 2 Extreme workstation at the Oak Ridge National Laboratory. Once $\tilde{h}_0(\tilde{z})$ is known, the top rod is impulsively set into motion and the computations are continued until h_{min}/R falls below a specified value, which is typically set to 10^{-3} unless otherwise specified.

Several tests are done to ensure the accuracy of the calculations. First, the volume of the liquid bridge

$$\frac{V}{R^3} = \pi \int_0^{L/R} \tilde{h}^2 \mathrm{d}\tilde{z} \tag{20}$$

is monitored throughout the computations. In all of the cases reported in this paper, the change in volume is always less than 0.01%. Second, the transient code was run with the disk velocity set equal to zero and by starting with an initial shape profile that is slightly perturbed from the equilibrium shape, namely $\tilde{h}_0(\tilde{z}) = \tilde{h}_0^{eq}(\tilde{z}) + h'(\tilde{z})$, where the superscript eq denotes the equilibrium shape and h' is the shape perturbation. In this manner, it was shown that static stability limits well known in the literature

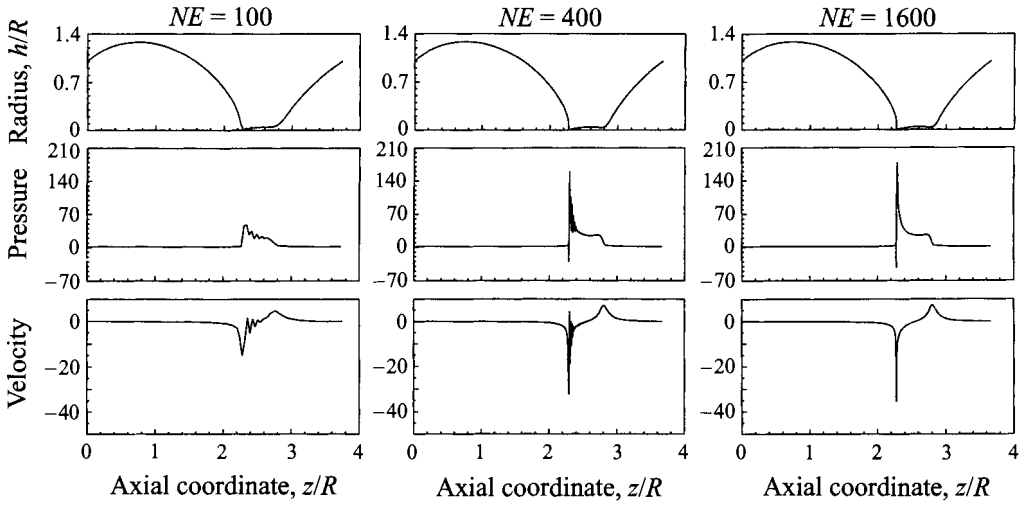

FIGURE 3. Convergence of computed values of the bridge profile and pressure and velocity fields with mesh refinement.

(Plateau 1863; Rayleigh 1879; Corriell *et al.* 1977) could be predicted with an accuracy better than 0.1%.

To study the sensitivity of computed solutions to mesh refinement, the domain was divided into NE uniformly spaced elements. Table 1 shows the sensitivity to mesh refinement of computed values of the dimensionless limiting length, L_d/R, which is the measure of the bridge extension when it breaks, and the resultant partial volume, V_l/V,

$$V_l/V = \frac{\pi \int_0^{h_{min}/R} \tilde{h}^2 \mathrm{d}\tilde{z}}{(V/R^3)}, \tag{21}$$

which is the ratio of the volume of the sessile drop that ends up on the lower disk upon bridge breakup to that of the entire bridge. The computational results shown are for the case in which the initial shape is that of a perfect cylinder of slenderness ratio $L_0/R = 3$, the motion is initiated by impulsively changing at time zero both the disk velocity and the gravitational Bond number from zero to $\tilde{U}_m = 0.028$ and $G = 0.342$, respectively, and setting $Oh = 2.932 \times 10^{-3}$. These dimensional parameters correspond to the situation in which the bridge liquid is water at 22.5°C, the disk radius $R = 0.16$ cm, and the disk velocity $U_m = 0.6$ cm s^{-1}. Figure 3 shows the variation with the dimensionless axial coordinate of the dimensionless interface shape function, dimensionless pressure (see (4)), and dimensionless axial velocity at the instant in time when $h_{min}/R = 0.004$ obtained with 100, 400, and 1600 elements. Figure 3 shows that the 100 element mesh does a good job of representing the interface shape everywhere except in the region where a liquid thread (neck or throat) connects the two halves of the bridge. In addition to the wiggles in the interface shape profile, large-amplitude oscillations are visible in the pressure and velocity profiles, which indicate that too few elements have been deployed in the tessellation. Oscillations in the interface shape profile have virtually disappeared but ones in the pressure and velocity profiles are still visible when the number of elements is increased to 400. As shown in figure 3, the computed values of all three quantities are devoid of spurious wiggles when the number of elements equals 1600. When the number

Number of elements, NE	L_d/R	V_1/V%
50	3.760	84.53
100	3.748	86.48
200	3.686	87.62
400	3.670	87.88
800	3.666	87.93
1600	3.665	87.94
3200	3.665	87.94

TABLE 1. Sensitivity of computed values of the limiting length, L_d/R, and partial volume, V_1/V, of a water bridge to mesh refinement. The parameters for which the computations have been carried out are stated in the text.

of elements is increased from 1600 to 3200, the maximum change in the computed values of the variables anywhere in the computational domain, including the pressure and velocity at the several large peaks that are visible in figure 3, is less than about 0.1%. Table 1 shows that computed values of both the limiting bridge length L_d/R and the partial volume V_l/V are changed less than 0.02% when the number of elements is increased from 800 to 1600. The results of figure 3 and table 1 make plain that although a couple of hundred uniformly spaced elements are adequate for obtaining values of $\tilde{h}$, L_d/R, and V_l/V, with about 0.5% accuracy, about five to ten times as many elements are required to obtain pressure and velocity fields everywhere inside the liquid bridge with the same accuracy. In addition to the accuracy tests described in this section, the accuracy of computational predictions is also compared to experimental measurements in §5 to ensure that the one-dimensional model is true to reality.

4. Experimental approach

The experiments have been designed to obtain quantitative information on the dynamics of stretching liquid bridges in order to compare the measurements with and verify the predictions of the one-dimensional model presented earlier. In the experiments, attention is paid in particular to the evolution in time of the shape of a stretching bridge as it is nearing breakup and the volume of the two supported drops that end up on the disks subsequent to the breakup of the bridge.

4.1. *Apparatus*

The liquid bridge is vertically confined or held captive between the parallel surfaces of two stainless steel, cylindrical disks or rods of equal radii that are coaxial with the bridge. The radii of the rods ranged between 0.08 and 0.32 cm in the experiments. The parallel surfaces of the rods are machined flat and perpendicular to the rod wall so that the liquid wets completely these surfaces and the three-phase contact lines of the bridge remain pinned on the sharp edges of the two faces. Fixing the contact lines during the stretching and breakup of a liquid bridge is important because experimental measurements show that the shape of the bridge and the distribution of liquid volume between the two faces subsequent to bridge breakup vary directly with the length, or circumference, of the contact lines. The upper rod is connected to a translation stage that is reassembled from a Harvard Apparatus syringe pump (Model 975) and allows the top rod to move upward at an adjustable, constant velocity of up to 0.6 cm s^{-1} while providing a sufficiently high ramping acceleration from a state

	ρ (g cm^{-3})	μ (g cm^{-1} s^{-1})	σ (g s^{-2})
Water	0.996	0.01	73.0
20% glycerol	1.048	0.018	72.4
50% glycerol	1.127	0.061	70.0
70% glycerol	1.182	0.299	68.5
85% glycerol	1.223	1.129	66.0
100% glycerol	1.262	14.99	63.0

TABLE 2. Physical properties of liquids and liquid–air interfaces in experiments

of rest to one of uniform translation. Hence, the time period that the translation stage takes to attain the desired constant velocity U_m is much shorter than the time period over which the bridge stretches and eventually breaks. The whole experimental apparatus, including parts to be described in what follows, is placed on a vibration isolation table from Newport.

The most important piece of equipment, which makes possible the wealth of quantitative experimental results to be presented in the next section, is a high-speed motion analysis/video system, the Kodak Ektapro Model EM 1012 Electronic Memory Motion Analyzer, and associated video hardware. The Ektapro system is composed of an intensified imager, i.e. the camera, and a processor which can record 1000 full images or 12 000 partial images per second.

Although the Ektapro stores the images digitally on a solid-state device, this information is subsequently transferred onto tape and replayed with a Panasonic model PV-54990 S-VHS recorder. Recorded images of transient bridge profiles are viewed on a Sony colour video monitor, model PVM-1341. Images of stretching bridges are then analysed in one of the two following ways. In the first of these, the images are digitized by means of a frame grabber, a Data Translation DT2851 board, that is installed in an IBM-compatible PC, and an edge detection routine is employed to locate the interfacial profile from the digitized images. Otherwise, the images are analysed with a similar capability that comes with the Ektapro system. Reassuringly, the two systems for image analysis have been shown to produce results that are in excellent agreement with each other. The image digitization systems allow rapid and accurate determination of the loci of liquid–gas interfaces from which the instantaneous shape of the bridge, i.e. L and h, and the volumes of the bridge and resultant drops are evaluated. Resolution of the digital images is typically 185 pixels cm^{-1} or larger, and the calibration is done with a resolution target, USAF-1951 by Newport. The typical bridge size is 0.2 cm or larger and can be measured within an error less than 3%, except when the bridge neck becomes vanishingly thin during its breakup. The volumes of axisymmetric bridges and resultant drops on the two rods are calculated by integrating their cross-sectional areas which are readily obtained from the loci of interface shapes. This volume measurement also provides an independent check for ensuring that the proper amount of liquid is actually being placed in the bridge (see below).

4.2. *Materials*

The bridge liquids used in the experiments are well recognized standards, e.g. triple-distilled water from Millipore Corp. and glycerol from EM Science in distilled water. Glycerol is used without further modification and dissolved in distilled water at the specified concentrations by weight. The physical properties of these liquid systems and

the surface tensions of these liquids in air at room temperature (see below) are given in table 2. The viscosity and density of water and glycerol solutions are taken from the literature (Timmermans 1960). The equilibrium surface tension of the liquid–air interfaces are measured using a pendant drop method (Harris & Byers 1989).

In the experiments carried out, the aqueous glycerol solutions with different concentrations have been chosen because of their desirable physical properties. Whereas the densities and surface tensions of these solutions are not very different from those of pure water, their viscosities can be made to vary by three orders of magnitude. Large variations in viscosity can result in significant differences in the evolution of the shapes of the bridges.

In the experiments, the measurements were taken within 8 hours of preparation of the solutions. All experiments were performed at the room temperature of $22° \pm 0.5°$C.

4.3. *Procedures*

The methodology of the experiments is straightforward. In a typical run, a bridge is formed by depositing a desired quantity of liquid by means of a calibrated Eppendorf pipette into the space between two rods that are separated by a certain initial distance from each other. Special care is taken to ensure that no air bubbles have been trapped inside the liquid bridge, eliminating any uncertainty in the bridge volume and shape. The bridge is then given a few minutes to approach a static equilibrium state. At the end of this period, the top rod is set into motion in the upward direction at the desired velocity and measurements of the instantaneous shape of the bridge are recorded continuously until the bridge breaks up and forms two drops that are pendant from and sessile on the two parallel faces of the rods. Since the process of bridge stretching and breakup is extremely repeatable, as verified in the experiments, the present technique provides a reliable picture of the dynamic evolution of the bridge shape. Reproducibility of results has been found to be within 3% by making measurements with the same liquid system under the same conditions but at different times.

4.4. *Ranges of dimensionless variables*

Experiments have been performed by systematically varying the geometric parameters, including the disk radius R, the initial length of the bridge L_0, the velocity of the upper disk U_m, and bridge volume V, *and* liquid physical properties and liquid–air surface tensions to gain insights into the effects of inertial, viscous, surface tension, and gravitational forces on the dynamics. The quantitative measurements to be reported in the next section have thus been made over wide ranges of the governing dimensionless groups. Namely, in what follows the Ohnesorge number is varied in the range of 2.1×10^{-3} to 5.9, the gravitational Bond number is varied in the range of 8.6×10^{-2} to 2, the dimensionless disk velocity is varied in the range of 1.3×10^{-3} to 4.8×10^{-2}, and the initial slenderness ratio is varied in the range of 1.75 to 3.5. Alternately, with U_m as the velocity scale, the Reynolds number is varied in the range of 2.7×10^{-3} to 19.1 and the capillary number is varied in the range of 5×10^{-6} to 1.4×10^{-1}.

5. Results and comparisons between computations and experimental measurements

Whereas it is straightforward in computations to vary any one dimensionless group while holding fixed all others, it is not possible to do so in laboratory experiments. Therefore, in what follows, most of the experimental results are presented in dimensional form. Nevertheless, the effects of all dimensional variables – rod radii R, liquid

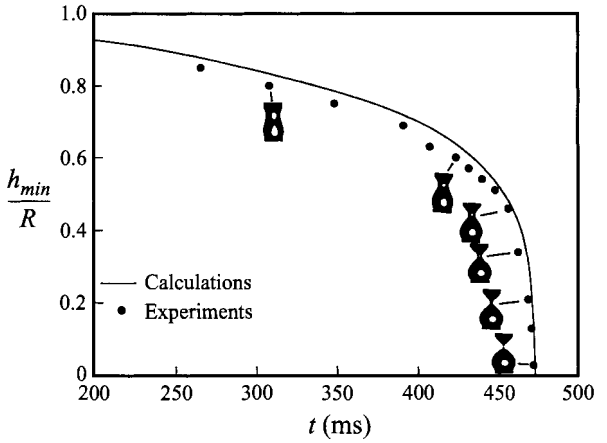

FIGURE 4. Evolution in time of the dimensionless minimum radius h_{min}/R of a water bridge of volume $V = 0.04$ cm^3 and initial slenderness ratio $L_0/R = 2$ that is held captive between two rods of radii $R = 0.16$ cm and is stretched at a velocity $U_m = 0.6$ cm s^{-1}.

volume V, velocity of the top rod U_m, initial bridge length L_0, and physical properties such as viscosity, surface tension, and density, μ, σ, and ρ, respectively – are studied quantitatively by both computational and experimental means in this section by systematically varying one of these variables while maintaining virtually all others fixed. However, computational results that show the effect of each one of the dimensionless groups on the dynamics of stretching bridges are also presented; these additional results help clarify and provide further insights into the dynamics. In what follows, continuous curves are used to denote results obtained from the numerical solution of the one-dimensional equations and points or filled circles denote experimental measurements.

5.1. *Bridge deformation and breakup*

Figure 4 shows the history of the deformation of a water bridge of volume $V = 0.04$ cm^3 and initial slenderness ratio $L_0/R = 2$ that is held captive between two rods of radii $R = 0.16$ cm that are separated from each other at a constant velocity $U_m = 0.6$ cm s^{-1}. Figure 4 depicts the evolution in time of both the dimensionless minimum neck radius, h_{min}/R, and bridge profile. It shows that good agreement exists between the experimental measurements and numerical calculations, with a maximum relative deviation in h_{min}/R of 7% between the measurements and the computations. This deviation is due primarily to the difficulty in experimentally measuring h_{min} as the neck radius tends to zero. Figure 4 shows that while the length of the liquid bridge increases linearly as time advances, $(L - L_0)/U_m = t$, the bridge initially deforms slowly, contracting at its middle portion and taking on a sequence of vase-like profiles as if minimizing its surface area. At longer times ($t > 450$ ms), however, when the length of the bridge has become sufficiently long, the neck starts to contract rapidly, resulting in a dramatic decrease in h_{min}/R with time. As the bridge approaches breakup, a liquid thread develops that connects the two large portions of liquid that are supported on the parallel faces of the two disks. During the final stages of breakup, the thread elongates while its radius, h_{min}, rapidly goes to zero. The elapsed time during this latter stage of bridge deformation is much shorter than the first stage and depends weakly on the operating parameters with a time scale of

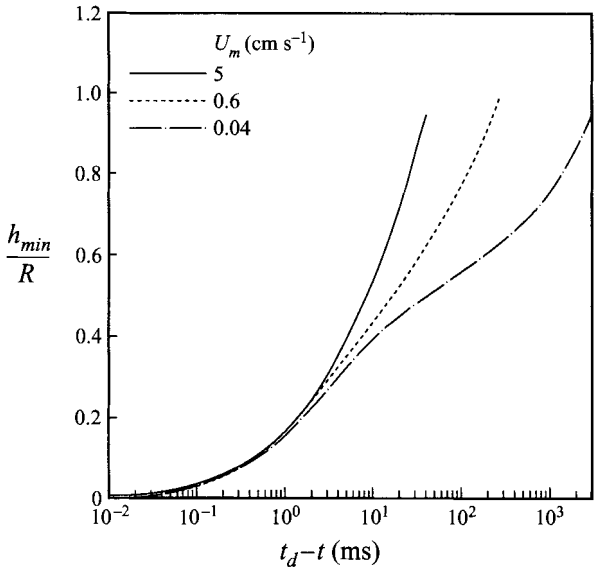

FIGURE 5. Evolution in time of the dimensionless minimum radius h_{min}/R of water bridges that are stretched at different velocities of $U_m = 0.04$, 0.6, and 5 cm s^{-1}. The bridge volume, the rod radii, and the initial slenderness ratio are identical in all three cases and are given by $V = 0.04$ cm^3, $R = 0.16$ cm, and $L_0/R = 2$, respectively. In figures 5 and 6, t_d denotes the time at the instant of bridge breakup.

about 20 ms or less. Selected instantaneous shapes of liquid bridges that are inserts to figure 4 and these two drastically different regimes of bridge deformation – a gradual one that lasts on the order of hundreds of milliseconds and a more catastrophic one that lasts on the order of tens of milliseconds – make plain the similarities between the problem of liquid bridge deformation and breakup and drop formation from capillaries in the dripping mode (cf. Zhang & Basaran 1995).

The weak dependence of the dynamics of the rapid elongation of bridges during their final stages of breakup on the operating parameters is made more apparent by figure 5 which shows calculated variations of h_{min}/R with time for three water bridges that are identical to each other in every respect except being subjected to different stretching velocities. Two things are done in figure 5 to better emphasize the period of bridge necking and breakup: first, time is measured backward from the instant when the bridge just breaks, $t_d - t$, with $t_d - t = 0$ standing for the instant of bridge breakup, and second, abscissa values are plotted as the logarithm of the transformed time. Figure 5 shows that within $t_d - t \sim 20$ ms, the curves depicting the variation of the minimum dimensionless bridge radius, h_{min}/R, with time for the three bridges being stretched at velocities differing by an order of magnitude collapse onto a single curve. The overlapping of the three curves of h_{min}/R versus time in figure 5 indicates that the profiles of the liquid threads evolve in a similar manner during the necking and breakup of the bridges regardless of the differences in the amounts of time taken by the bridges to break and the lengths attained by them prior to their breakup. The dependence of the maximum length attained by a bridge on its stretching velocity is discussed in detail in §5.2.

Figure 6 shows the change with time of the axial location along the bridge at which its radius h is a minimum, l/R (see figure 2), for the three bridges of figure 5. The axial location measured from the bottom stationary rod at which the radius h is a

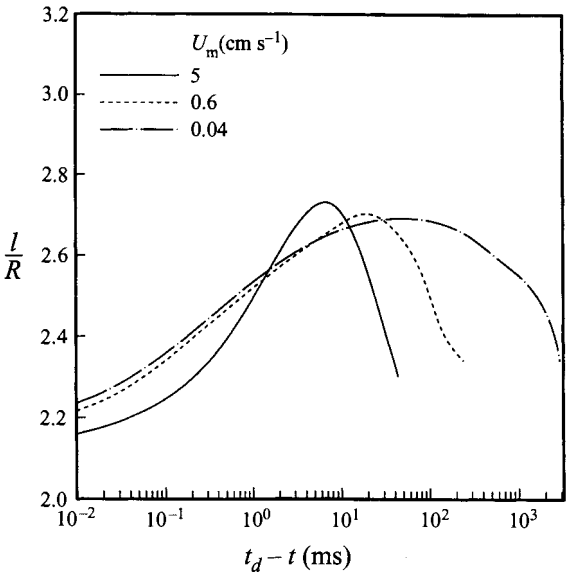

FIGURE 6. Evolution in time of the dimensionless axial location at which the bridge radius is a minimum l_{min}/R of water bridges that are stretched at different velocities of $U_m = 0.04$, 0.6, and 5 cm s^{-1}. The bridge volume, the rod radii, and the initial slenderness ratio are identical in all three cases and are given by $V = 0.04$ cm^3, $R = 0.16$ cm, and $L_0/R = 2$, respectively.

minimum is found to increase initially as the portion of the liquid adjacent to the upper moving rod is pulled up with it. Figure 6 also shows that l/R subsequently attains a maximum and then decreases rapidly until the bridge breaks at $t_d - t = 0$. The rapid fall of l/R with time as $t \to t_d$ coincides with the development of a mass of virtually stagnant liquid that is sessile on the lower stationary rod and contracts its surface area to take on a nearly spherical profile (cf. figure 4).

Further insights into the final stages of bridge deformation can be gained by examining the pressure and velocity distributions inside a bridge at the incipience of breakup. Figure 7 shows the interface shape, dimensionless pressure (equation (4)), and dimensionless axial velocity inside a water bridge under the same conditions as the bridge of figure 4. Figure 7 shows that aside from a thin liquid thread, two localized regions of extremely large pressure and velocity have developed as the fluid interface is about to rupture. First, in the vicinity of the axial coordinate where h is a minimum and the lower portion of the thread joins the virtually spherical mass of liquid that is sessile on the lower rod, with increasing value of the axial coordinate the mean curvature successively takes on a large positive value $\tilde{\mathscr{P}}^I_{max}$, a large negative value $\tilde{\mathscr{P}}_{min}$, and then another large positive value $\tilde{\mathscr{P}}^{II}_{max} \gg \tilde{\mathscr{P}}^I_{max}$. The first positive peak occurs at $\tilde{z} = \tilde{z}^I_{max} \approx 2.218 < l/R$, where $\tilde{\mathscr{P}}^I_{max} = 11.45$. The minimum value of the pressure, $\tilde{\mathscr{P}}_{min} = -67.52$, is attained just below the axial location where $h = h_{min}$ and $\partial\tilde{h}/\partial\tilde{z} = 0$, $\tilde{z} = \tilde{z}_{min} \approx 2.222$. Just above the location where h is a minimum, at $\tilde{z} = \tilde{z}^{II}_{max} \approx 2.229$, the pressure profile exhibits a positive peak, $\tilde{\mathscr{P}}^{II}_{max} = 185.49$, which is the absolute largest pressure inside the liquid bridge at this instant in time. Figure 7 also shows that a second localized zone of large pressures is just starting to develop at the upper end of the liquid thread where it joins the mass of liquid that is pendant from the upward moving top rod. The velocity profile shown in figure 7 provides further information on the details of the breakup process. First, the large

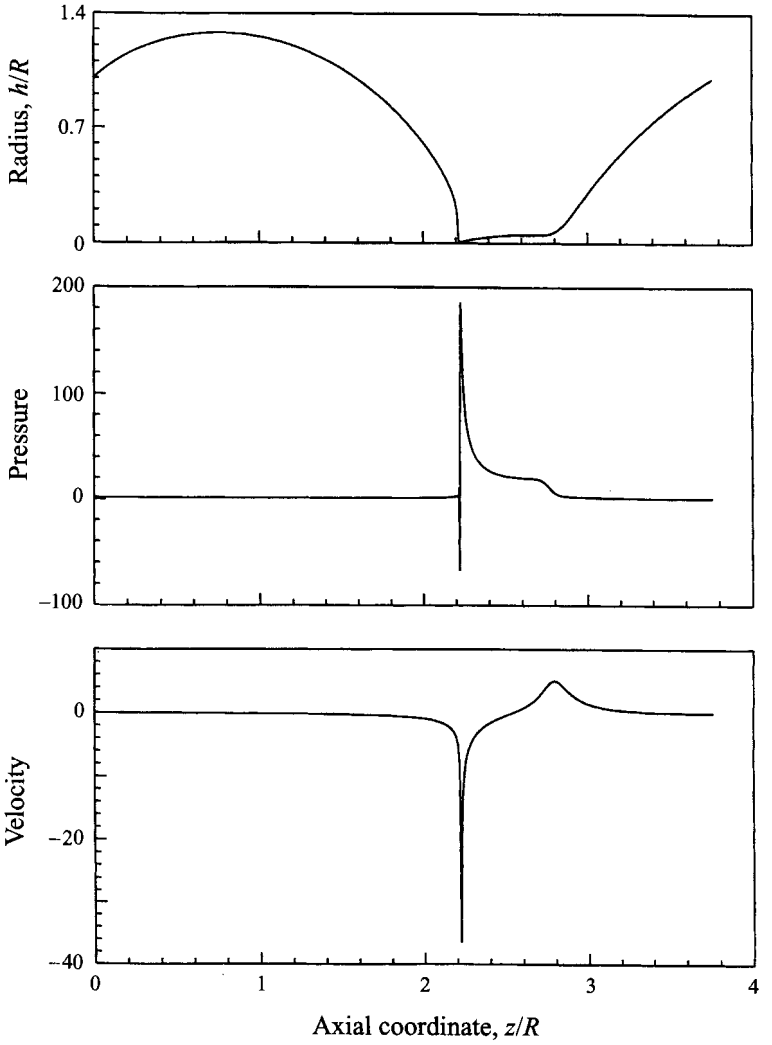

FIGURE 7. Variation of the dimensionless bridge radius h/R, pressure $\tilde{\mathscr{P}}$, and axial velocity $\tilde{v}$ with axial position inside a water bridge of volume $V = 0.04$ cm^3 and initial slenderness ratio $L_0/R = 2$ that is held captive between two rods of radii $R = 0.16$ cm and is stretched at a velocity $U_m = 0.6$ cm s^{-1}. Here $\tilde{t} = 62.89$ and $h_{min}/R = 3.96 \times 10^{-3}$.

and negative peak in the velocity profile, $\tilde{v}_{min} = -36.53$, in the vicinity of the location where h is a minimum and the thread joins the sessile drop, signals a net downward movement of liquid out of the thread and into the sessile drop. Second, the smaller and positive peak in the velocity profile, $\tilde{v}_{max} = 5.04$, in the vicinity of the location where the thread joins the pendant drop, signals a net upward movement of liquid out of the thread and into the pendant drop. The interface shape and velocity and pressure profiles show that the thread will break at its bottom end first whereas the velocity profile makes clear that there is a net loss of liquid and an accompanying thinning of the thread as the water bridge nears breakup. The latter observation is confirmed by examination of interface shapes and velocity profiles over several time steps close to breakup. Although locally large gradients in velocity can give rise to large viscous contributions to the total pressure, the capillary contribution to the

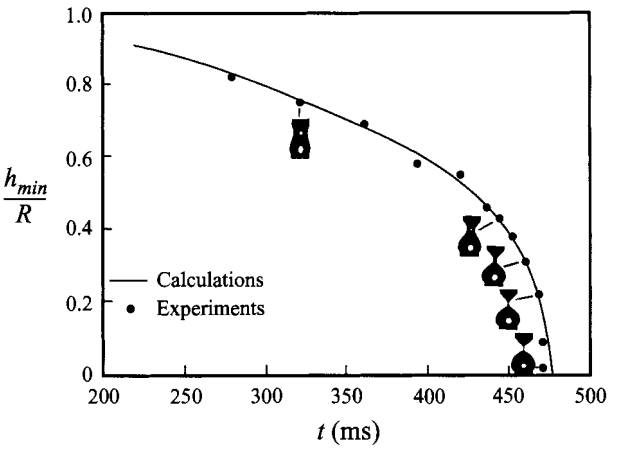

FIGURE 8. Evolution in time of the dimensionless minimum radius h_{min}/R of a bridge of a solution of 85% glycerol in water of volume $V = 0.04$ cm^3 and initial slenderness ratio $L_0/R = 2$ that is held captive between two rods of radii $R = 0.16$ cm and is stretched at a velocity $U_m = 0.6$ cm s^{-1}.

pressure $\tilde{\mathscr{P}}$ dominates the viscous contribution to it for the case of the breaking water bridge shown in figure 7. Whereas the viscous contribution to the pressure ranges between -11 and 16.86, the capillary contribution ranges between -74.38 and 191.68 (cf. equation (4)).

It is observed in the experiments that immediately after the thread breaks at its lower end, the now freed end of the thread is accelerated in the upward direction by the unbalanced force of surface tension and rolls up to take on a bulbous profile (Peregrine, Shoker & Symon 1990). The water thread of figures 7 and 4 is sufficiently short at breakup and moves upward with a sufficiently large speed after breakup that it collides with and merges with the upper pendant mass of liquid without forming any satellite droplets.

Figure 8 shows the history of the deformation of a bridge of an 85% glycerol solution of volume $V = 0.04$ cm^3 and initial slenderness ratio $L_0/R = 2$ that is held captive between two rods of radii $R = 0.16$ cm that are separated from each other at a constant velocity $U_m = 0.6$ cm s^{-1}. Figure 8 depicts the evolution in time of both the dimensionless minimum neck radius, h_{min}/R, and bridge profile. Like figure 4, figure 8 shows that good agreement exists between the experimental measurements and the numerical calculations. Although the bridge of the 85% glycerol solution shows a dynamic response that is qualitatively similar to that of a water bridge, it exhibits a thread that is longer and lasts longer than that of a water bridge on account of the larger viscosity of the former bridge.

Figure 9 shows the interface shape, dimensionless pressure (equation (4)), and dimensionless axial velocity inside the bridge of the 85% glycerol solution whose history of deformation is depicted in figure 8 as it is nearing breakup. Comparison of figures 9 and 7 reveals that the details of the dynamics of the breakup of a bridge of an 85% glycerol solution are drastically different from those of a water bridge. Figure 9 makes plain that while liquid is flowing out of the thread at both of its ends, liquid is also accumulating in the middle of the thread. In contrast to the breakup of the water bridge discussed previously, the bridge of an 85% glycerol solution breaks so that the two ends of its thread separate from the top and bottom portions of the bridge virtually at the same instant in time. The result of this sequence of events is

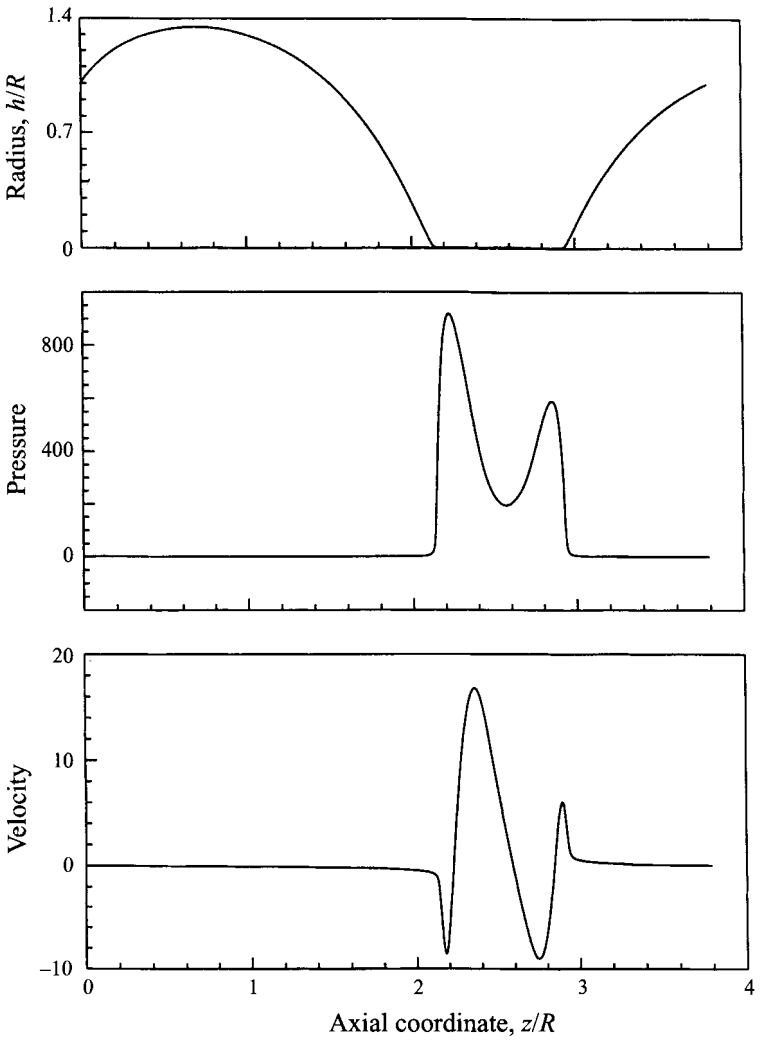

FIGURE 9. Variation of the dimensionless bridge radius h/R, pressure $\tilde{\mathscr{P}}$, and axial velocity $\tilde{v}$ with axial position inside a bridge of a solution of 85% glycerol in water of volume $V = 0.04$ cm^3 and initial slenderness ratio $L_0/R = 2$ that is held captive between two rods of radii $R = 0.16$ cm and is stretched at a velocity $U_m = 0.6$ cm s^{-1}. Here $\tilde{t} = 54.35$ and $h_{min}/R = 1.01 \times 10^{-3}$.

the creation of a small satellite droplet that occupies the region between the two large liquid masses that are pendant and sessile on the two rods.

It is instructive to determine the conditions for transition from breakup of the thread at its lower end to nearly simultaneous breakup at both of its ends. When the concentration of glycerol is increased to 20%, it is found that although the thread is now slightly longer than that of water, the thread again breaks first at its bottom end and no satellite is formed (not shown). Figure 10 shows the interface shape, dimensionless pressure (equation (4)), and dimensionless axial velocity inside a bridge of a 50% glycerol solution as it is nearing breakup. There are two obvious differences between the breakup of a bridge of a 50% glycerol solution and that of bridges of water and 20% glycerol solution. First, the mean curvature is positive everywhere along the interface of the former bridge. Second, the velocity goes through zero at

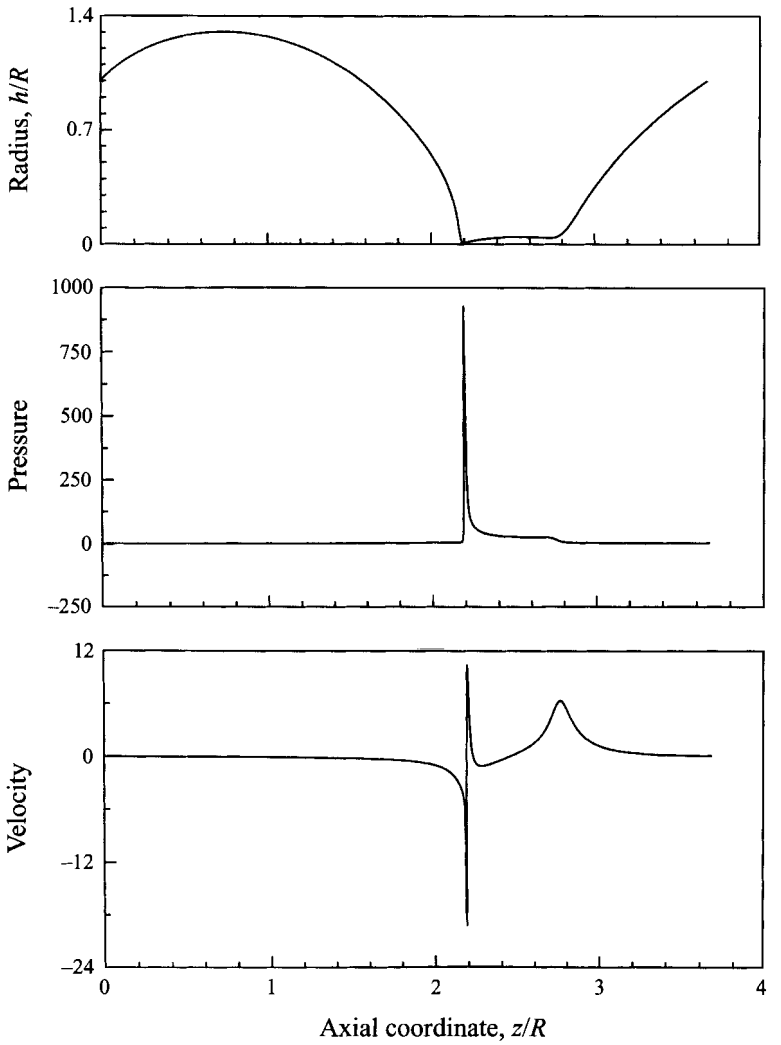

FIGURE 10. As for figure 9 but for a bridge of a solution of 50% glycerol in water. Here $\tilde{t} = 55.18$ and $h_{min}/R = 1.01 \times 10^{-3}$.

h_{min}. Therefore, experiments show that the lower end, although it breaks first, is not accelerated in the upward direction as rapidly as in the case of the lower-viscosity bridges. On account of the lower speed of the freed end of the thread, the upper end of the thread can break before the upward moving thread merges with the liquid mass that is pendant from the top rod. However, the satellite that is thereby produced is too small to be followed in time with the current experimental setup where the camera is focused on the entire bridge. The fate of the satellite, if desired, can of course be readily determined by focusing on or magnifying the liquid thread albeit at the expense of ignoring the dynamics away from this region.

The aforementioned dynamics of satellite drops are akin to ones observed in the formation of drops from capillaries in a gravitational field (Zhang & Basaran 1995) and deformation and breakup of free drops in low Reynolds number flow (Stone, Bentley & Leal 1986). Zhang & Basaran (1995) have shown that when the thread

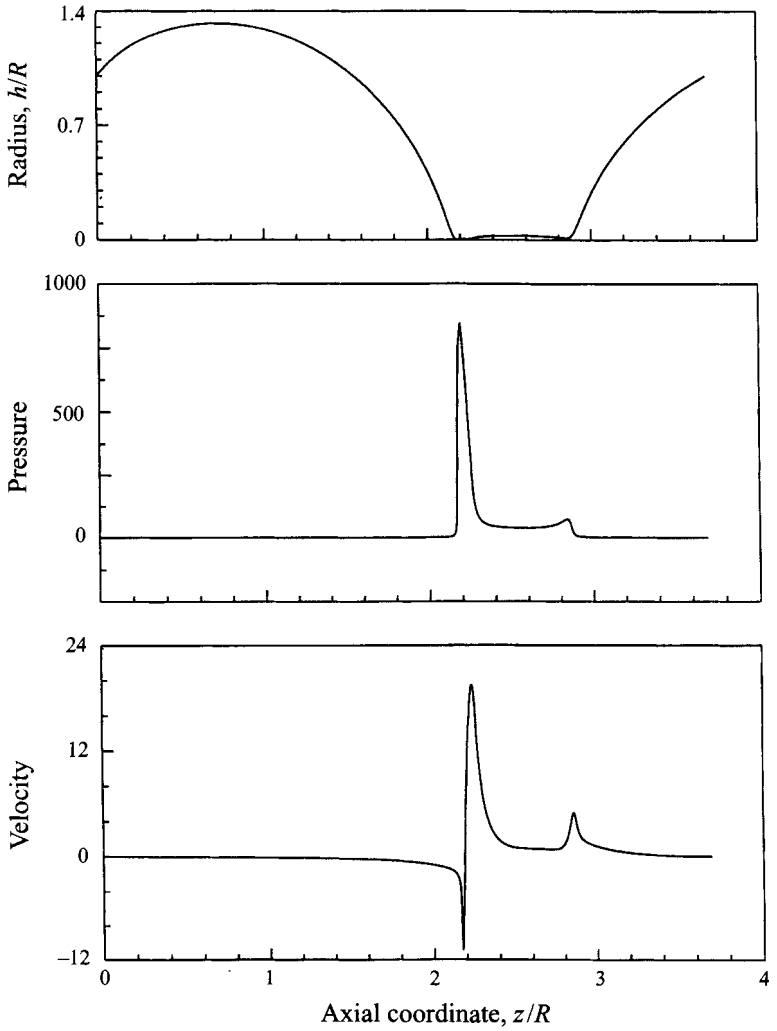

FIGURE 11. As for figure 9 but for a solution of 70% glycerol in water. Here $\tilde{t} = 53.96$ and $h_{min}/R = 1.03 \times 10^{-3}$.

breaks first at its bottom end and then at its top end, the dynamics of the resultant satellite droplet is complex. The satellite collides with the pendant drop and then either merges with or bounces off it.

Figure 11 shows the interface shape, dimensionless pressure, and dimensionless axial velocity inside a bridge of a 70% glycerol solution as it is nearing breakup. Figure 11 and the experiments show that similar to the case of a bridge of an 85% glycerol solution, the two ends of the thread in this situation too break virtually at the same time. A blow up of the regions localized around the threads in these two cases (not shown) reveals that the thread length increases but the maximum thickness of the thread decreases as the glycerol concentration increases from 70% to 85%.

Figure 12 shows the interface shape, dimensionless pressure, and dimensionless axial velocity inside a bridge of pure glycerol as it is nearing breakup. First, it is noteworthy that as viscosity is increased by two orders of magnitude in going from figure 7 to figure 9 and then by another order of magnitude in going from figure 9

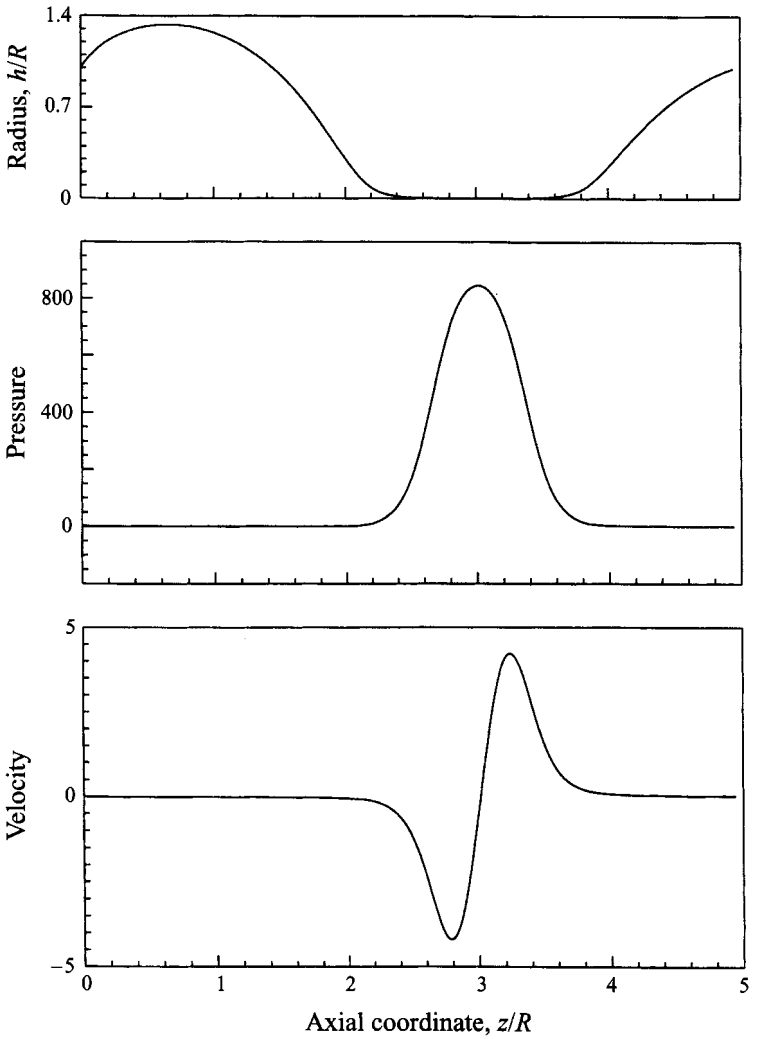

FIGURE 12. As figure 9 but for a pure glycerol bridge. Here $\tilde{t} = 86.64$ and $h_{min}/R = 1.02 \times 10^{-3}$.

to figure 12 that the localized but large variations in $\tilde{h}$, $\tilde{\mathscr{P}}$, and $\tilde{v}$ occur over larger distances. Second, comparison of figure 12 to figures 7 and 9–11 demonstrates the role played by increasing viscosity in delaying the breakup of the liquid thread: plainly, the thread length increases as viscosity increases. Third, in contrast to both the water bridge and the bridges of 20, 50, 70, and 85% glycerol solutions, figure 12 and the experiments show that the thread of the pure glycerol bridge breaks by rupturing at its middle. Figure 12 also shows that the interface profile and the pressure field are virtually symmetric and the velocity field is virtually antisymmetric about the midpoint of the thread of a pure glycerol bridge nearing breakup, a result that accords with the analytical theory of breakup of thin jets under Stokes flow conditions recently developed by Papageorgiou (1995*a*). The experiments show that once the thread breaks at its middle, the broken ends roll toward and merge with the two supported drops, without forming a satellite drop.

L_0/R	L_d/R	$V_1/V(\%)$
1.75	3.763	86.49
2.00	3.761	86.52
2.50	3.761	86.51
2.75	3.761	86.54
3.00	3.764	86.52
3.25	3.760	86.54
3.50	3.761	86.54

TABLE 3. Effect of initial dimensionless length or slenderness ratio, L_0/R, of a bridge on its dimensionless limiting length, L_d/R, and partial volume, V_1/V. Here the bridge liquid is water, $R = 0.16$ cm, $U_m = 0.6$ cm s^{-1}, and $V = 0.039$ cm^3. The solutions have been obtained with 1000 uniformly spaced elements.

5.2. *Limiting length of a bridge*

Although the results presented in §5.1 make plain that certain features of the dynamics of stretching liquid bridges remain qualitatively similar from one situation to the next, nevertheless (*a*) there are quantitative differences between certain other features of the dynamics and (*b*) the volume of break-off drops, that is the sessile and the pendant drops which result upon the breakup of the liquid bridge, vary considerably as some of the parameters are varied. The differences in dynamic response under different operating conditions are particularly striking during the period of bridge necking and breakup and, hence this subsection summarizes the variation of the limiting length of liquid bridges, L_d, as a function of the relevant parameters.

Unless otherwise pointed out, all of the results presented in this subsection have been obtained for bridges whose initial lengths equal twice the rod radii, namely $L_0 = 2R$. This is because it has been found from both experimental measurements and numerical calculations that the initial length (so long as it falls within the stable region), has a negligible effect on the salient features of the dynamics of bridge stretching and breakup. By way of example, computational results shown in table 3 demonstrate that both the limiting bridge length and partial volume vary by less than about 0.1% as the initial length of a water bridge of $V = 0.04$ cm^3 that is stretched at $U_m = 0.6$ cm s^{-1} is varied from $1.75R$ to $3.5R$.

Figure 13 shows the variation of the dimensionless limiting length L_d/R of liquid bridges of mixtures of glycerol and water as a function of the mass fraction of glycerol. The results shown have been obtained holding fixed the rod radii, the velocity of the upper rod, and the bridge volume at $R = 0.16$ cm, $U_m = 0.6$ cm s^{-1}, and $V = 0.04$ cm^3, respectively. Indeed, one can ascertain from figure 13 the composite effects of the forces due to surface tension, viscosity, and gravity on the stretching and breakup of liquid bridges by the changes in surface tension, viscosity, and density experienced by the bridge liquid as the glycerol concentration is varied. It is worth recalling that as the glycerol concentration increases, the surface tension falls while the density and viscosity rise (cf. table 2). It is well known for static bridges that surface tension and density play opposite roles in determining bridge stability on account of the manner in which these two parameters affect the gravitational Bond number $G = \rho R^2 g/\sigma$ (see Coriell *et al.* 1977). Namely, the maximum length of a stable bridge rises (falls) as the value of the surface tension (density) rises. Viscosity, on the other hand, plays a great role in prolonging the existence of a stretching bridge by damping or even eliminating surface waves that arise on the rapidly stretching interface. These

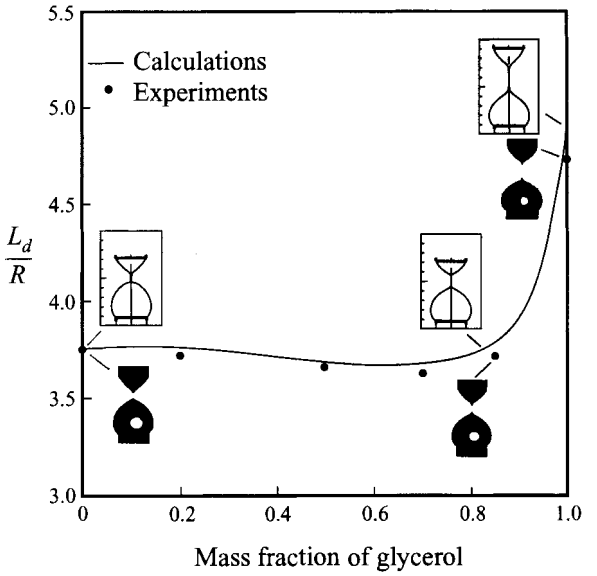

FIGURE 13. Dimensionless limiting length L_d/R of bridges of mixtures of water and glycerol as a function of the mass fraction of glycerol. Here $V = 0.04$ cm^3, $L_0/R = 2$, $R = 0.16$ cm, and $U_m = 0.6$ cm s^{-1}.

stabilizing and inhibiting effects of high viscosity have already been demonstrated through the discussion accompanying figures 7 and 9–12 and are further illustrated by the photograph inserts to figure 13. Hence, changes in surface tension and density caused by increasing the glycerol concentration reduce the limiting length L_d of the bridge whereas the rise in the viscosity caused by increasing the glycerol concentration increases L_d by increasing the length of the liquid thread of the bridge. Therefore, under the competition between these opposing effects of viscosity, density, and surface tension, it accords with intuition that the limiting length of a stretching bridge should attain a minimum when the concentration of the glycerol solutions reaches a critical value. In the case shown in figure 13, the minimum is reached when the bridge liquid consists of a water–glycerol mixture whose glycerol concentration lies between 50 and 70%. For solutions of higher concentrations of glycerol, the viscosity of the liquid is sufficiently high to inhibit the growth of surface perturbations and thereby allow the existence of longer and thinner threads. It is noteworthy that for a bridge of pure glycerol the thread extends over a distance exceeding two times the rod radius before it breaks, which results in a significant increase in the limiting length of the bridge. Based on studies of drop formation from capillaries (Zhang & Basaran 1995), yet even longer threads are expected to occur as the disk velocity increases. For example, these authors found that for drops of solutions of 85% glycerol in water, the thread length can exceed three times the capillary radius when the average velocity of the liquid in the capillary becomes sufficiently large and approaches that at which transition from dripping to jetting takes place. The effect of the disk velocity on the limiting length of liquid bridges is discussed in detail later in this paper.

Table 2 shows that while the surface tension and density of glycerol–water solutions vary by 14% and 26%, respectively, as the concentration of glycerol varies from 0 to 100%, the viscosity of these solutions varies by more than three orders of magnitude over the same concentration range. These trends provide an alternative way of

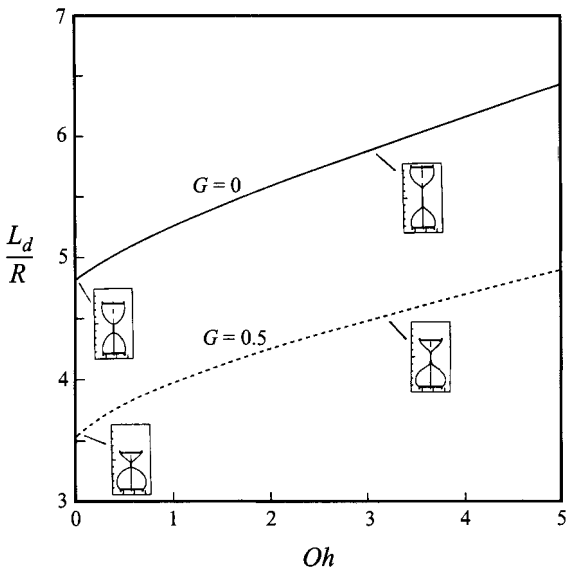

FIGURE 14. Computational predictions of the dimensionless limiting length L_d/R of bridges as a function of the Ohnesorge number Oh at two different gravitational Bond numbers, $G = 0.0$ and 0.5. Here $V/R^3 = 3\pi$, $\tilde{U}_m = 0.028$, and $L_0/R = 3$ for $G = 0$ and $L_0/R = 2$ for $G = 0.5$.

viewing the results of Figure 13. Over this concentration range, the gravitational Bond number varies as $0.34 \leqslant G \leqslant 0.50$ and the dimensionless disk velocity varies as $0.028 \leqslant \tilde{U}_m \leqslant 0.034$, and therefore, given the much wider range over which the Ohnesorge number varies, $3 \times 10^{-3} \leqslant Oh \leqslant 4.2$, one can think of the results of figure 13 as showing the variation of L_d/R with Oh while virtually holding fixed both G and $\tilde{U}_m$.

Figure 14 shows computational predictions of the variation of the dimensionless limiting bridge length L_d/R as a function of the Ohnesorge number Oh at two different values of the gravitational Bond number G holding fixed the dimensionless disk velocity at $\tilde{U}_m = 0.028$ and the dimensionless volume at $V/R^3 = 3\pi$. Figure 14 makes it possible to compare two situations, one where gravitational force is quite important relative to surface tension force, $G = 0.5$, and the other where gravity is absent, $G = 0$. Figure 14 makes plain that the limiting length of a stretching bridge increases monotonically as the Ohnesorge number increases due primarily to the increasing importance of viscous forces over surface tension forces in making possible the realizability of longer threads. As expected, a stretching bridge deforms symmetrically about $\tilde{z} = L/2R$ in the absence of gravity, $G = 0$. Figure 15 shows that when $G = 0$ and surface tension forces dominate viscous forces, $Oh = 0.1$, the thread simultaneously breaks at both of its ends. Increasing G while holding Oh fixed destroys the symmetry of the bridge profile and causes the thread to break at its lower end first, as shown in figure 14. However, regardless of the value of G, figure 14 shows that the thread breaks at its middle when viscous forces dominate surface tension ones.

Figure 16 shows computational predictions of the variation of the dimensionless limiting bridge length L_d/R as a function of the gravitational Bond number G at two different values of the Ohnesorge number Oh holding fixed the dimensionless disk velocity at $\tilde{U}_m = 0.028$ and the dimensionless volume at $V/R^3 = 3\pi$. Evidently,

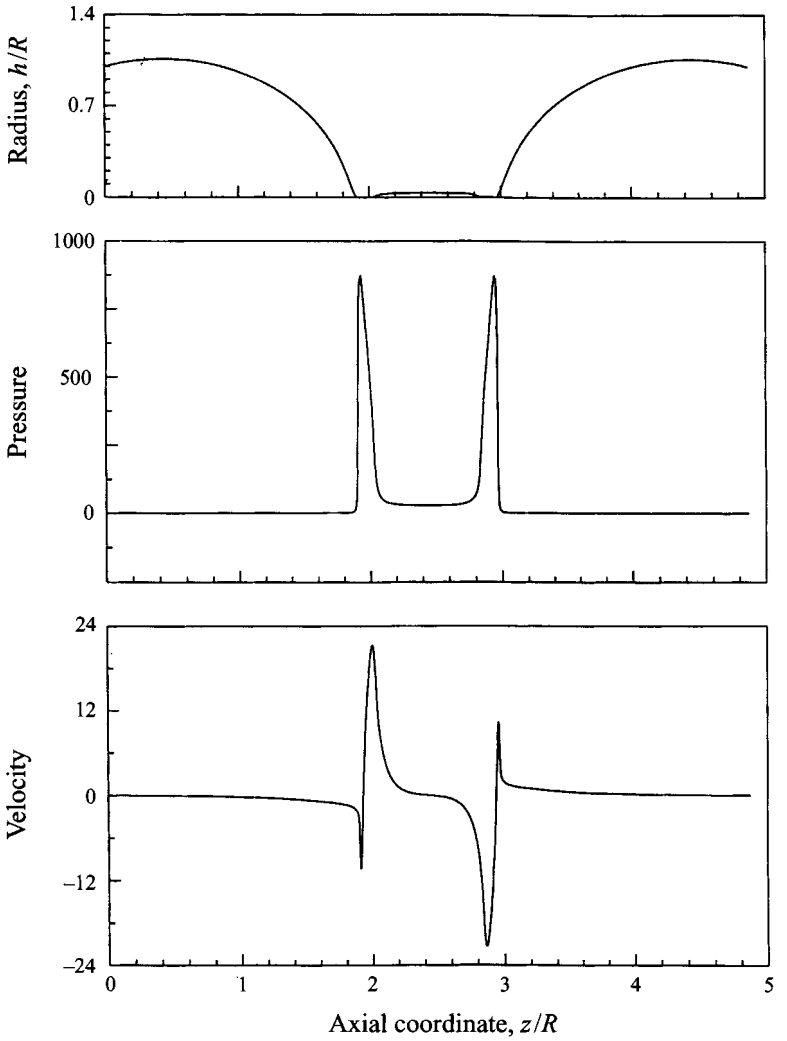

FIGURE 15. Variation of the dimensionless bridge radius h/R, pressure $\tilde{\mathscr{P}}$, and axial velocity $\tilde{v}$ with axial position inside an initially cylindrical bridge of initial slenderness ratio $L_0/R = 3$ and dimensionless volume $V/R^3 = 3\pi$ in the absence of gravity $G = 0$ and with $Oh = 0.1$ and $\tilde{U}_m = 0.028$. Here $\tilde{t} = 66.83$ and $h_{min}/R = 1.03 \times 10^{-3}$.

similar to static liquid bridges (see, e.g., Coriell *et al.* 1977), the limiting length of a bridge decreases as the gravitational Bond number increases. In addition, the inserts to figure 16 show that the shapes and the volumes of the two drops that are supported on the upper and the lower rods change substantially as G changes, a point to which we return below.

Because the surface tensions and densities of bridges of mixtures of water and glycerol can at most be varied by about 26% (see table 2), the gravitational Bond number is most readily changed in the experiments by varying the radii of the supporting rods. Figure 17 compares experimental measurements and theoretical predictions of the variation of the dimensionless limiting length L_d/R with the rod radius R for water bridges of volume $V = 2\pi R^3$ that are stretched at a velocity of $U_m = 0.6$ cm s^{-1}. By varying the rod radius over the wide range 0.05 cm $\leqslant R \leqslant$ 0.5 cm

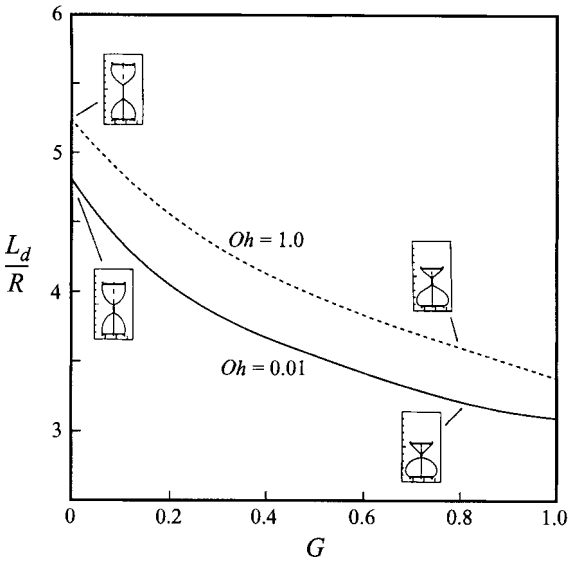

FIGURE 16. Computational predictions of the dimensionless limiting length L_d/R of bridges as a function of the gravitational Bond number G at two different Ohnesorge numbers, $Oh = 0.01$ and 1.0. Here $V/R^3 = 3\pi$, $\tilde{U}_m = 0.028$, and $L_0/R = 3$ for $G = 0$ and $L_0/R = 2$ for $G > 0$.

in figure 17, the gravitational Bond number is varied from 3.3×10^{-2} to 3.4, while the Ohnesorge number and the dimensionless disk velocity vary slightly between 5.2×10^{-3} and 1.7×10^{-3} and 0.016 and 0.050, respectively. Figure 17 shows that as the bridge volume and the length of its thread increase with increasing rod radius, the dimensional limiting length of the bridge, L_d, increases monotonically with it while the dimensionless limiting length, or the limiting slenderness ratio, L_d/R, shows the opposite trend and decreases monotonically with increasing rod radius. Figure 17 shows that over the interval 0.08 cm $< R <$ 0.32 cm, the dimensionless limiting length decreases essentially linearly with increasing R. For bridges with $R > 0.32$ cm, however, the larger gravitational force, which scales as R^3, compared to the surface tension force, which scales as R^2, causes most of the bridge liquid to accumulate inside the liquid body that is sessile on the lower rod (see also §5.3) while the volume of the liquid cone hanging from the upper rod relative to R^3 decreases considerably. This decrease in the relative volume of the cone as R increases results in the shape of the cone changing gradually from convex to concave (see the photograph inserts to figure 17). As in the case of drop formation from capillaries of large radii (see Zhang & Basaran 1995), following the first breakup of the thread at its lower point the concave shape of the cone and the accompanying increase in the thickness of the thread conspire to lower the local mean curvature at the upper part of the thread which considerably delays its breakup there. Therefore, in this case, the satellite droplet generated subsequent to thread breakup is found to be quite large and eventually falls in the direction of gravity and coalesces with the drop that is sessile on the lower rod.

Figure 18 compares experimental measurements and theoretical predictions of the variation of the dimensionless limiting length L_d/R as a function of the bridge volume V scaled by πR^3 for water bridges that are captured between two rods of $R = 0.16$ cm and stretched at a velocity of $U_m = 0.6$ cm s^{-1}. Figure 18 shows that with increasing bridge volume, the amount of liquid that ends up on the lower portion of the bridge

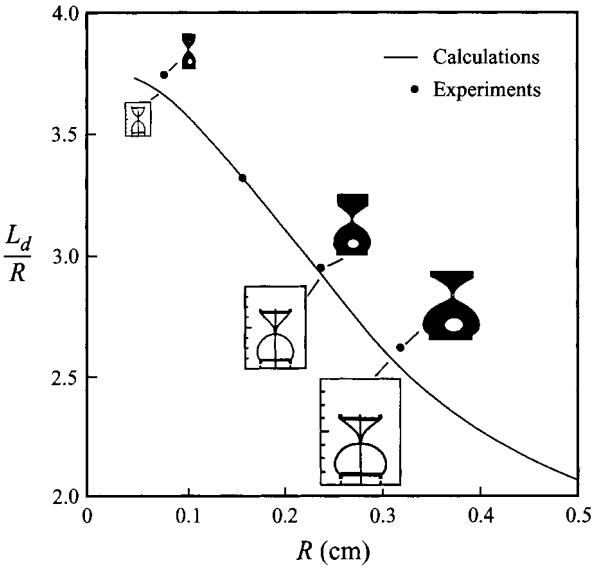

FIGURE 17. Dimensionless limiting length L_d/R of water bridges as a function of the rod radius R. Here $L_0/R = 2$ and $U_m = 0.6$ cm s^{-1}.

increases relative to that on the upper portion of the bridge, a finding that accords with intuition. Although the sizes of both portions of the bridge increase as the bridge volume increases, the length of the thread connecting the two portions remains virtually unchanged. Therefore, the increase in the limiting bridge length is due solely to the increase in the sizes of the pendant and the sessile drops. The rate of change of the limiting length with bridge volume is significant when the bridge volume is small but levels off as the volume becomes large.

When a liquid bridge is axially stretched at a low velocity, the shape that the bridge assumes at each instant in time closely resembles the equilibrium shape that it would have were the moving disk instantaneously brought to rest and sufficient time were to elapse for the transients in the bridge profile and velocity and pressure fields to die down due to the action of viscosity. Indeed, in this slow mode of stretching, the limiting length that the bridge attains exceeds the maximum stable length of a static bridge by only a small amount. By contrast, at higher stretching velocities the departure of the transient shapes from the equilibrium shapes is large so that the breakup of the bridge is delayed significantly and its limiting length is increased substantially over the maximum stable length of a static bridge. Figure 19 exhibits the increase in the limiting length L_d/R with increasing stretching velocity U_m for water bridges of $V = 0.04$ cm^3 and $R = 0.16$ cm. The rate of increase of the limiting length with U_m is low at low stretching velocities but becomes significant when $U_m > 1$ cm s^{-1} due to the increasing importance of inertial force over surface tension force as measured by the dimensionless disk velocity. It is noteworthy that as the stretching speed increases, the liquid cone hanging from the upper rod shows a small increase in volume while becoming greatly elongated whereas the lower portion of the bridge liquid shows a small decrease in volume while exhibiting an absence of visible variation in shape (see the inserts to figure 19 and §5.3). Additionally, the thread length is found to increase as U_m increases. Both of these effects conspire to accelerate the rate of increase of the limiting length of the bridge as the stretching velocity increases.

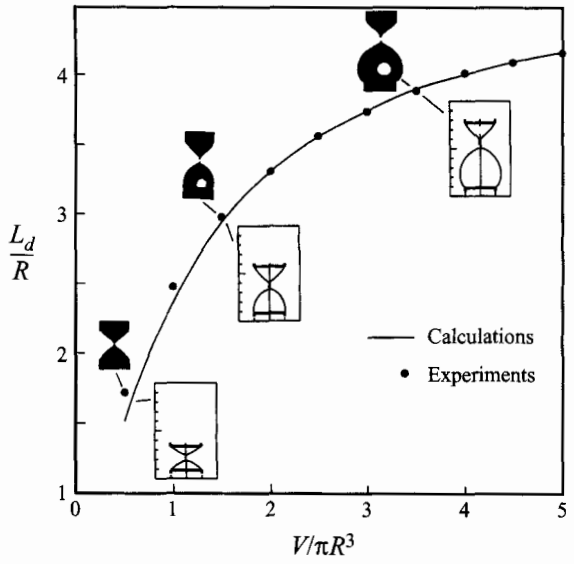

FIGURE 18. Dimensionless limiting length L_d/R of water bridges as a function of the dimensionless bridge volume divided by π, $V/\pi R^3$. The initial slenderness ratio L_0/R equals the abscissa value for $V/\pi R^3 < 3$ and it equals 3 for $V/\pi R^3 \geqslant 3$. The rod radius and disk velocity are held fixed at $R = 0.16$ cm and $U_m = 0.6$ cm s^{-1}, respectively.

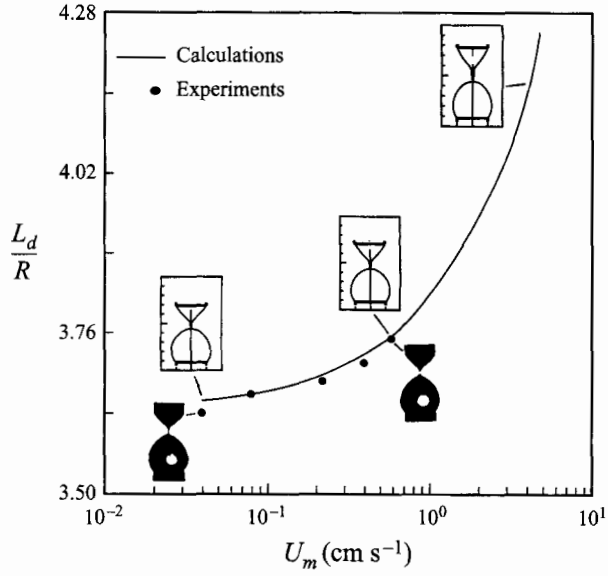

FIGURE 19. Dimensionless limiting length L_d/R of water bridges as a function of the rod velocity U_m. Here $V = 0.04$ cm^3, $L_0/R = 2$, and $R = 0.16$ cm.

Although disk velocities in excess of 0.6 cm s^{-1} are impossible to attain in the laboratory with the present setup, the fate of liquid bridges at large stretching velocities is explored here with the aid of the numerical model. Figure 20 shows the effect of increasing disk velocity on the instantaneous shape of water bridges of $V = 0.04$ cm^3 captured between two rods of $R = 0.16$ at the moment when they

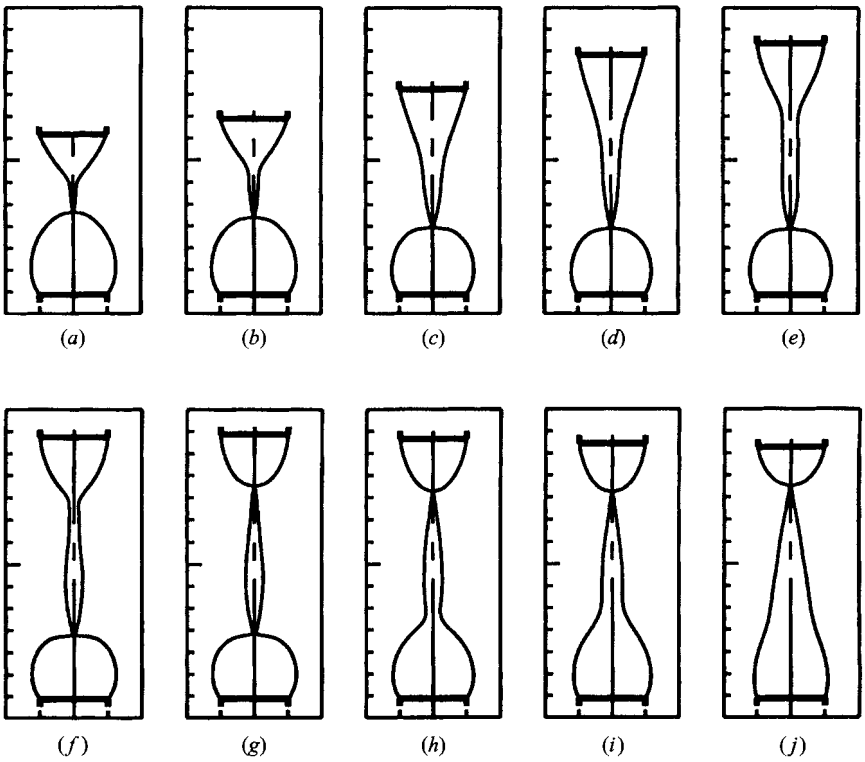

FIGURE 20. Computed limiting shapes of water bridges of volume $V = 0.04$ cm^3 held captive between two rods of radii $R = 0.16$ cm at the instants when they are about to break as a function of rod velocity in cm s^{-1}: (*a*) $U_m = 5$, (*b*) $U_m = 10$, (*c*) $U_m = 15$, (*d*) $U_m = 20$, (*e*) $U_m = 25$, (*f*) $U_m = 25.8$, (*g*) $U_m = 26.1$, (*h*) $U_m = 26.5$ (*i*) $U_m = 27$, and (*j*) $U_m = 30$.

are about to break. The computational results depicted in figure 20 show that the limiting bridge length increases dramatically as the disk velocity increases from 5 to 25 cm s^{-1}, reaches a maximum value when $U_m = 26.1$ cm s^{-1}, and decreases at larger disk velocities. The striking increase in the limiting length for 5 cm s^{-1} $\leqslant U_m \leqslant$ 25 cm s^{-1} is clearly due to the increase in the thread length. As a result of the large thread, one or more large satellite drops would be expected to be created subsequent to the thread breakup (cf. Zhang & Basaran 1995). Perhaps even more interesting are the changes in the evolution in time of the bridge shape for disk velocities near this maximum and the manner of bridge breakup with increasing disk velocity. As discussed in §5.1, when $U_m \ll 25.8$ cm s^{-1}, the thread of a water bridge consistently breaks first at its lower end (see also figure 20*a–f*) due to the larger capillary pressure that develops there on account of the larger curvature of the interface in the vicinity of where $h = h_{min}$. However, as the disk velocity continues to increase over a critical value, which equals 26.1 cm s^{-1} in this case, the liquid cone hanging from the upper rod moves upward so rapidly that it breaks from the rest of the bridge before the lower portion of the liquid attached to the bottom rod can assume a spherical profile and lead to the breakup of the lower end of the thread. Evidently, at the critical disk velocity, which equals the disk velocity at which L_d/R is a maximum, the thread breaks at its two ends simultaneously, as shown in figure 20(*g*). This remarkable switch in the

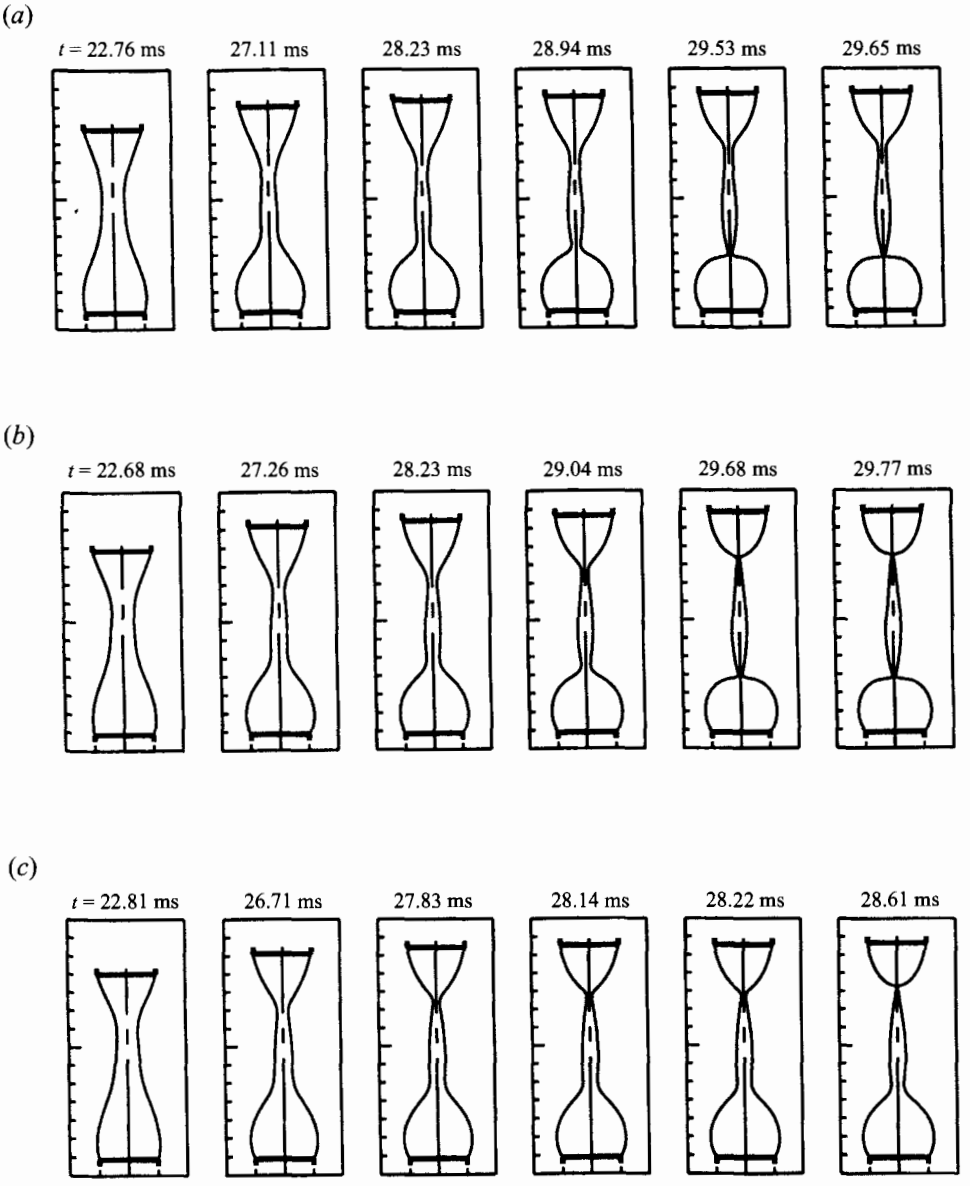

FIGURE 21. The effect of rod velocity on the deformation history of water bridges with emphasis on the time period close to and at breakup: (*a*) $U_m = 25.8$ cm s^{-1}, (*b*) $U_m = 26.1$ cm s^{-1}, and (*c*) $U_m = 26.5$ cm s^{-1}. Here the bridges have volume $V = 0.04$ cm^3 and are held captive between two rods of radii $R = 0.16$ cm.

breakup sequence is explicitly demonstrated in figure 21 by showing details of the shape evolutions of three water bridges that are being stretched at $U_m = 25.8$, 26.1 and 26.5 cm s^{-1}, corresponding to figure 20(*f,g,h*), respectively. Zhang & Basaran (1996) have recently reported a similar switch in the breakup sequence of liquid threads in drop formation from capillaries in the presence of an electric field.

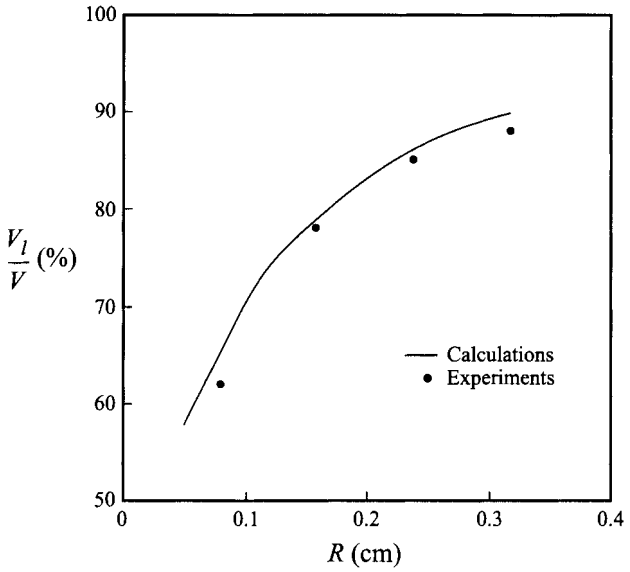

FIGURE 22. Partial volume V_l/V of water bridges as a function of rod radius R. Here the initial slenderness ratio and the disk velocity are held fixed at $L_0/R = 2$ and $U_m = 0.6$ cm s^{-1}, respectively.

5.3. *Partial volumes of liquid bridges*

Figure 22 shows experimental measurements and computational predictions of the variation of the partial volume as a function of the radii of the two rods. Here the liquid is water, the rods are separated at a fixed velocity of $U_m = 0.6$ cm s^{-1}, and the bridge volume $V = 2\pi R^3$. By varying the rod size from $R = 0.08$ cm to 0.32 cm, the gravitational Bond number in figure 22 is varied by a factor of 16. Figure 22 shows that the partial volume V_l/V increases as the relative importance of gravity to surface tension force increases. This finding accords with intuition because as the relative importance of gravitational force increases by using rods of increasing radii, more liquid accumulates on the bottom portion of the bridge before breakup (cf. figure 17). Figure 22 shows that the error incurred in the computational prediction of the partial volume relative to the experimentally measured value is larger than that incurred in the prediction of the limiting length of bridges. The larger errors between computed and measured values of partial volume are attributable to the larger errors that are made in the experimental determination of the bridge profile $h(z)$ which is then integrated to calculate the experimental value of V_l/V. Nevertheless, the maximum difference between the predicted and the experimentally measured value of partial volume is still smaller than 4%.

Figure 23 shows experimental measurements and computational predictions of the variation of the partial volume as a function of the total bridge volume V scaled by πR^3. Here the liquid is again water, the radii of the rods are kept constant at $R = 0.16$ cm, and the rods are separated at a fixed velocity of $U_m = 0.6$ cm s^{-1}. As $V/\pi R^3$ increases, the importance of the force of gravity relative to that of surface tension increases: this enlarges the volume of the sessile drop prior to bridge breakup (cf. figure 18) and, therefore, increases the partial volume. It is noteworthy that the rate of increase of the partial volume due to an increase in the gravitational force caused

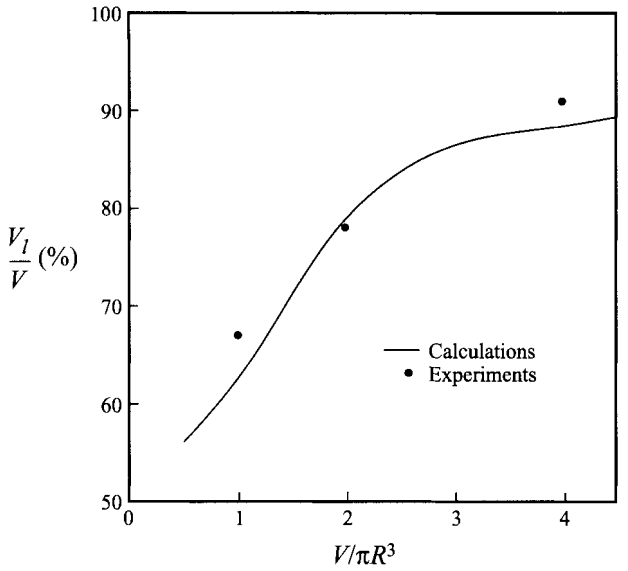

FIGURE 23. Partial volume V_l/V of water bridges as a function of the dimensionless volume of the bridges divided by π, $V/\pi R^3$. The initial slenderness ratio L_0/R equals the abscissa value for $V/\pi R^3 < 3$ and it equals 3 for $V/\pi R^3 \geqslant 3$. Here the disk radii and the disk velocity are held fixed at $R = 0.16$ cm and $U_m = 0.6$ cm s^{-1}, respectively.

by using either rods of larger radii (cf. figure 22) or liquid bridges of larger volumes (cf. figure 23) slows and approaches an asymptote as R or $V/\pi R^3$ becomes large.

Whereas the rod velocity has a big influence on the limiting length of liquid bridges, figure 24 shows that it has a small influence on their partial volumes. The computational results shown in figure 24 are for water bridges of volume $V = 0.04$ cm^3 that are held captive between rods of radii $R = 0.16$ cm. Owing to the increase in the volume of and the elongation suffered by the liquid cone hanging from the upper rod as the disk velocity increases (cf. the inserts to figure 19), the volume enclosed by the lower portion of the bridge decreases slightly as U_m increases. Consequently, the partial volume of the bridges are found to decrease by only 8.5% as the rod velocity increases from 0.04 cm s^{-1} to 5 cm s^{-1}. Moreover, as shown in figures 20 and 21, if the disk velocity is sufficiently large, the liquid thread and the satellite droplets that they give rise to can enclose volumes that are not negligible compared to those of the pendant and the sessile drops. Investigation of the fate and volume of the satellite droplets in this situation is left open as problems for future research.

Figure 25 shows the effect of glycerol mass fraction on the partial volume of liquid bridges. The computational results shown have been obtained for bridges of fixed volume $V = 0.04$ cm^3 held captive between disks of radii $R = 0.16$ cm that are separated from each other at a constant velocity of $U_m = 0.6$ cm s^{-1}. First, it is noteworthy that the variation of V_l/V as a function of the glycerol concentration is the opposite of the variation of L_d/R as a function of glycerol concentration presented in figure 13, namely the curves in figures 25 and 13 are, qualitatively speaking, virtually vertical reflections of each other. Here, as in figure 13, the physical properties of the bridge liquid play an interesting role in setting the variation of the partial volume with the glycerol mass fraction. At low glycerol concentrations, the partial volume increases with increasing concentration because the response is controlled by an increase in the importance of the force of gravity relative to that

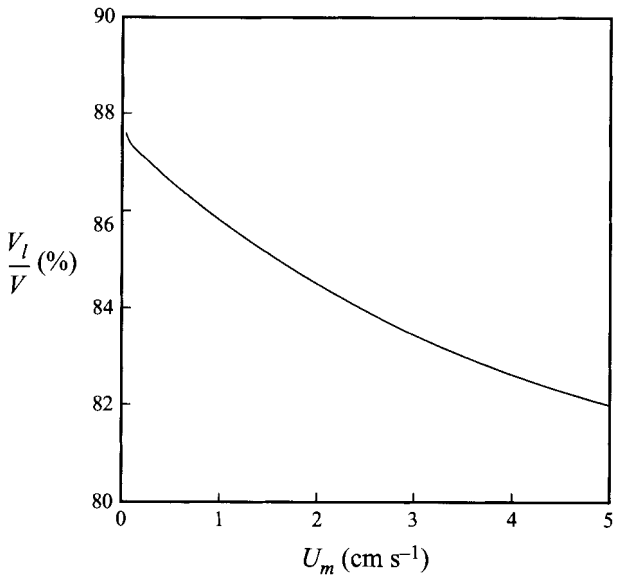

FIGURE 24. Computed values of the partial volume V_l/V of water bridges as a function of the rod velocity U_m. Here the drop volume and the initial slenderness ratio are held fixed at $V = 0.04$ cm^3 and $L_0/R = 2$, respectively.

of surface tension due to the accompanying increase in the density of the bridge liquid. At large glycerol concentrations, however, the response is determined by the dimensionless disk velocity which increases as the glycerol concentration increases and causes the partial volume to decrease.

6. Concluding remarks

In this paper, we have probed through both theoretical and experimental means the effects of inertial, viscous, gravitational, and surface tension forces on the dynamics of stretching liquid bridges. According to the foregoing results, the maximum or limiting length that a stretching liquid bridge attains at breakup increases significantly with increasing liquid viscosity and increasing stretching velocity. By contrast, the maximum slenderness ratio that a bridge can attain prior to breaking decreases significantly as rod radius increases. Subsequent to the breakup of a bridge, two large drops are generated such that one is pendant from the top moving rod and the other is sessile on the stationary bottom rod. Evidently, the manner in which the bridge volume is distributed between these two drops is a strong function of the relative importance of viscous, inertial, and gravitational forces to surface tension forces.

The interface dynamics studied in some detail in this paper clearly has implications in other applications. In particular, one motivation for the present work comes from the desire to improve our understanding of drop formation from capillaries because stretching liquid bridges provide a convenient way to subject a liquid thread to a well-controlled extension. Recently, Zhang & Basaran (1996) have carried out a detailed study of the dynamics of drop formation in the presence of an electric field. These authors have shown that when the field strength exceeds a critical value, the mode of thread breakup switches from its bottom to its top. Among other things, one consequence of increasing the field strength is that it increases the speed with

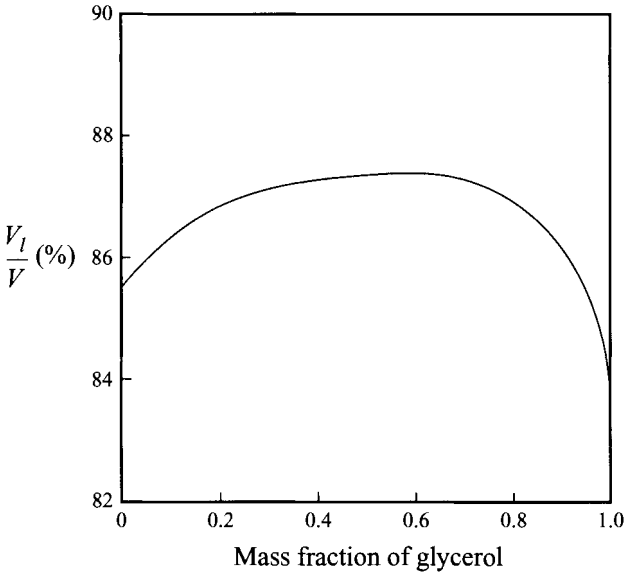

FIGURE 25. Computed values of the partial volume V_l/V of bridges of glycerol-water mixtures as a function of the mass fraction of glycerol. Here the drop volume, the initial slenderness ratio, and the disk velocity are held fixed at $V = 0.04$ cm^3, $L_0/R = 2$, and $U_m = 0.6$ cm s^{-1}, respectively.

which a liquid thread is stretched. Therefore, the present computations make plain that the mechanism of the switching of thread rupture observed in experiments on drop formation in electric fields is due to the rise of the ratio of inertial forces to surface tension forces beyond some critical value.

The use of the one-dimensional model to simulate the dynamics of the entire bridge deformation and breakup process hinges on the slender jet approximation being valid throughout the motion. However, comparison of computational results with experimental measurements shows that while the agreement between the two is excellent with respect to the limiting length of the bridge, a relatively larger deviation between the two arises with respect to the partial volume of bridges after breakup. Recently, Schulkes (1993*a*) has examined the validity of one-dimensional models based on the inviscid slice model (Lee 1974) and the Cosserat continuum without viscosity (Green 1976) by comparing their predictions to ones obtained from two-dimensional potential flow calculations carried out with the boundary integral method in the problem of the breakup of a stationary liquid bridge. Schulkes has shown that the one-dimensional models are in general ill-suited to describe the dynamics of *inviscid* liquid bridges as they near breakup. Therefore, a goal of future research is to examine the dynamics of the breakup of stretching liquid bridges with fully two-dimensional models with viscosity using the Galerkin/finite element method (cf. Basaran & DePaoli 1994).

Electric fields can be used to stabilize non-stretching liquid bridges and thereby allow them to attain much longer lengths prior to breakup (Gonzalez *et al.* 1989; Sankaran & Saville 1993). An extensive study of the effects of an externally applied electric field on the dynamics of the deformation and breakup of stretching liquid bridges is also underway in our laboratory. When an electric field is imposed parallel to the axis of symmetry of a bridge of a dielectric liquid, both the limiting length and the partial volume of the bridge increase as the field strength increases. By contrast,

when the electric field is applied perpendicular to the axis of symmetry of the bridge, the electric field plays a destabilizing role and the limiting length of a bridge decreases as the field strength increases.

This work was supported by the Division of Chemical Sciences, Office of Basic Energy Sciences, US Department of Energy under contract DE-AC05-96OR22464 with Lockheed Martin Energy Research Corp. (X.Z., R.S.P., O.A.B.), New Directions in Chemical Engineering Program of the School of Chemical Engineering of Purdue University and its Industrial Partners (O.A.B.), and the Exxon Education Foundation (O.A.B.).

REFERENCES

ANILKUMAR, A. V., GRUGEL, R. N., SHEN, X. F., LEE, C. P. & WANG, T. G. 1993 Control of thermocapillary convection in a liquid bridge by vibration. *J. Appl. Phys.* **73**, 4165-4170.

BASARAN, O. A. 1992 Nonlinear oscillations of viscous liquid drops. *J. Fluid Mech.* **241**, 169–198.

BASARAN, O. A. & DEPAOLI, D. W. 1994 Nonlinear oscillations of pendant liquid drops. *Phys. Fluids* **6**, 2923–2943.

BORKAR, A. & TSAMOPOULOS, J. 1991 Boundary-layer analysis of the dynamics of axisymmetric capillary bridges. *Phys. Fluids* A **3**, 2866–2874.

BROWN, R. A. 1988 Theory of transport processes in single crystal growth from the melt. *AIChE J.* **34**, 881–911.

BROWN, R. A. & SCRIVEN, L. E. 1980 The shapes and stability of captive rotating drops. *Phil. Trans. R. Soc. Lond.* A **297**, 51–79.

CHEN, T.-Y. & TSAMOPOULOS, J. 1993 Nonlinear dynamics of capillary bridges: theory. *J. Fluid Mech.* **255**, 373–409.

CHEN, T.-Y., TSAMOPOULOS, J. A. & GOOD, R. J. 1992 Capillary bridges between parallel and non-parallel surfaces and their stability. *J. Colloid Interface Sci.* **151**, 49–69.

CORIELL, S. R., HARDY, S. C. & CORDES, M. R. 1977 Stability of liquid zones. *J. Colloid Interface Sci.* **60**, 126–136.

DENN, M. M. 1980 Drawing of liquids to form fibers. *Ann. Rev. Fluid Mech.* **12**, 365–387.

EGGERS, J. & DUPONT, T. F. 1994 Drop formation in a one-dimensional approximation of the Navier–Stokes equation. *J. Fluid Mech.* **262**, 205–221.

ENNIS, B. J., LI, J., TARDOS, G. I. & PFEFFER, R. 1990 The influence of viscosity on the strength of an axially strained pendular liquid bridge. *Chem. Engng Sci.* **45**, 3071–3088.

FOWLE, A. A., WANG, C. A. & STRONG, P. F. 1979 Experiments on the stability of conical and cylindrical liquid columns at low Bond numbers. In *Proc. 3rd European Symp. Mat. Sci. Space*, pp. 317–325.

GAUDET, S., MCKINLEY, G. H. & STONE, H. A. 1994 Extensional deformation of Newtonian and non-Newtonian liquid bridges in microgravity. *AIAA* 94-0696, pp. 1–9.

GILLETTE, R. D. & DYSON, D. C. 1971 Stability of fluid interfaces of revolution between equal solid circular plates. *Chem. Engng J.* **2**, 44–54.

GONZALEZ, H., MCCLUSKEY, F. M. J., CASTELLANOS, A. & BARRERO, A. 1989 Stabilization of dielectric liquid bridges by electric fields in the absence of gravity. *J. Fluid Mech.* **206**, 545–561.

GREEN, A. E. 1976 On the non-linear behaviour of fluid jets. *Intl J. Engng Sci.* **14**, 49–63.

GRESHO, P. M., LEE, R. L. & SANI, R. C. 1979 On the time-dependent solution of the incompressible Navier–Stokes equations in two and three dimensions. In *Recent Advances in Numerical Methods in Fluids* (ed. C. Taylor & K. Morgan), vol. 1, pp. 27–79. Pineridge, Swansea.

HARRIS, M. T. & BYERS, C. H. 1989 An advanced technique for interfacial tension measurement in liquid-liquid system. *Oak Ridge National Laboratory/TM*-10734.

HAYNES, J. M. 1970 Stability of a fluid cylinder. *J. Colloid Interface Sci.* **32**, 652–654.

JOHNSON, M., KAMM, R. D., HO, L. W., SHAPIRO, A. & PEDLEY, T. J. 1991 The nonlinear growth of surface-tension-driven instabilities of a thin annular film. *J. Fluid Mech.* **233**, 141–156.

KHESHGI, H. S. 1989 Profile equations for film flows at moderate Reynolds numbers. *AIChE J.* **35**, 1719–1727.

KHESHGI, H. S. & SCRIVEN, L. E. 1983 Penalty finite element analysis of unsteady free surface flows. In *Finite Elements in Fluids* (ed. R. H. Gallagher, J. T. Oden, O. C. Zienkiewicz, T. Kawai & M. Kawahara), vol. 5, pp. 393–434. Wiley.

KISTLER, S. F. & SCRIVEN, L. E. 1983 Coating flows. In *Computational Analysis of Polymer Processing* (ed. J. R. A. Pearson & S. M. Richardson), pp. 243–299. Applied Science Publishers.

KROGER, R., BERG, S., DELGADO, A. & RATH, H. J. 1992 Stretching behavior of large polymeric and Newtonian liquid bridges in plateau simulation. *J. Non-Newtonian Fluid Mech.* **45**, 385–400.

KROGER, R. & RATH, H. J. 1995 Velocity and elongation rate distributions in stretched polymeric and Newtonian liquid bridges. *J. Non-Newtonian Fluid Mech.* **57**, 137–153.

LAPIDUS, L. & PINDER, G. F. 1982 *Numerical Solution of Partial Differential Equations in Science and Engineering*. John Wiley.

LEE, H. C. 1974 Drop formation in a liquid jet. *IBM J. Res. Dev.* **18**, 364–369.

LUSKIN, M. & RANNACHER, R. 1982 On the smoothing property of the Crank-Nicholson scheme. *Applicable Anal.* **14**, 117–135.

MASON, G. 1970 An experimental determination of the stable length of cylindrical liquid bubbles. *J. Colloid Interface Sci.* **32**, 172–176.

MESEGUER, J. 1983 The breaking of axisymmetric slender liquid bridges. *J. Fluid Mech.* **130**, 123–151.

MESEGUER, J. & PERALES, J. M. 1991 A linear analysis of *g*-jitter effects on viscous cylindrical liquid bridges. *Phys. Fluids* A **3**, 2332–2336.

MESEGUER, J. & SANZ, A. 1985 Numerical and experimental study of the dynamics of axisymmetric slender liquid bridges. *J. Fluid Mech.* **153**, 83–101.

MICHAEL, D. H. 1981 Meniscus stability. *Ann. Rev. Fluid Mech.* **13**, 189–215.

MILLER, C. A. & SCRIVEN, L. E. 1968 The oscillations of a droplet immersed in another fluid. *J. Fluid Mech.* **32**, 417–435.

MOLLOT, D. J., TSAMOPOULOS, J., CHEN, T.-Y. & ASHGRIZ, A. 1993 Nonlinear dynamics of capillary bridges: experiments. *J. Fluid Mech.* **255**, 411–435.

PAPAGEORGIOU, D. T. 1995*a* On the breakup of viscous liquid threads. *Phys. Fluids* **7**, 1529–1544.

PAPAGEORGIOU, D. T. 1995*b* Analytical description of the breakup of liquid jets. *J. Fluid Mech.* **301**, 109–132.

PATZEK, T. W. & SCRIVEN, L. E. 1982 Capillary forces exerted by liquid drops caught between crossed cylinders: A 3-D meniscus problem with free contact line. In *Proc. 2nd Intl Colloq Drops Bubbles* (ed. D. H. Le Croissette), pp. 308–314. JPL Publication 82-7, Jet Propulsion Laboratory, Pasadena, California.

PERALES, J. M. & MESEGUER, J. 1992 Theoretical and experimental study of the vibration of axisymmetric viscous liquid bridges. *Phys. Fluids* A **4**, 1110–1130.

PEREGRINE, D. H., SHOKER, G. & SYMON, A. 1990 The bifurcation of liquid bridges. *J. Fluid Mech.* **212**, 25–39.

PLATEAU, J. 1863 Experimental and theoretical researches on the figures of equilibrium of a liquid mass withdrawn from the action of gravity. In *Annual Report of the Board of Regents of the Smithsonian Institution*, pp. 270–283. Washington, DC.

RAYLEIGH, Lord 1879 On the instability of jets. *Proc. Lond. Math. Soc.* **10**, 4–13.

RUSCHAK, K. J. 1978 Flow of a falling film into a pool. *AIChE J.* **24**, 705–709.

RUSSO, M. J. & STEEN, P. H. 1986 Instability of rotund capillary bridges to general disturbances: Experiment and theory. *J. Colloid Interface Sci.* **113**, 154–163.

SANKARAN, S. & SAVILLE, D. A. 1993 Experiments on the stability of a liquid bridge in an axial electric field. *Phys. Fluids* A **5**, 1081–1083.

SANZ, A. 1985 The influence of the outer bath in the dynamics of axisymmetric liquid bridges. *J. Fluid Mech.* **156**, 101–140.

SANZ, A. & DIEZ, J. L. 1989 Non-axisymmetric oscillations of liquid bridges. *J. Fluid Mech.* **205**, 503–521.

SCHULKES, R. M. S. M. 1993*a* Nonlinear dynamics of liquid columns: a comparative study. *Phys. Fluids* A **5**, 2121–2130.

SCHULKES, R. M. S. M. 1993*b* Dynamics of liquid jets revisited. *J. Fluid Mech.* **250**, 635–650.

SHIPMAN, R. W. G., DENN, M. M. & KEUNINGS, R. 1991 Mechanics of the "falling plate" extensional rheometer. *J. Non-Newtonian Fluid Mech.* **40**, 281–288.

SRIDHAR, T., TIRTAATMADJA, V., NGUYEN, D. A. & GUPTA, R. K. 1991 Measurement of extensional viscosity of polymer solutions. *J. Non-Newtonian Fluid Mech.* **40**, 271–280.

STONE, H. A., BENTLEY, B. J. & LEAL, L. G. 1986 An experimental study of transient effects in the breakup of viscous drops. *J. Fluid Mech.* **173**, 131–158.

STRANG, G. & FIX, G. J. 1973 *An Analysis of the Finite Element Method.* Prentice-Hall.

STRANI, M. & SABETTA, F. 1988 Viscous oscillations of a supported drop in an immiscible fluid. *J. Fluid Mech.* **189**, 397–421.

TIMMERMANS, J. 1960 *The Physico-Chemical Constants of Binary Systems in Concentrated Solutions*, vol. 4. Interscience.

TIRTAATMADJA, V. & SRIDHAR, T. 1993 A filament stretching device for measurement of extensional viscosity. *J. Rheol.* **37**, 1081–1102.

TSAMOPOULOS, J., CHEN, T.-Y. & BORKAR, A. 1992 Viscous oscillations of capillary bridges. *J. Fluid Mech.* **235**, 579–609.

UNGAR, L. H. & BROWN, R. A. 1982 The dependence of the shape and stability of captive rotating drops on multiple parameters. *Phil. Trans. R. Soc. Lond.* A **306**, 347–370.

ZHANG, Y. & ALEXANDER, J. I. D. 1990 Sensitivity of liquid bridges subject to axial residual acceleration. *Phys. Fluids* A **2**, 1966–1974.

ZHANG, X. & BASARAN, O. A. 1995 An experimental study of dynamics of drop formation. *Phys. Fluids* **7**, 1184–1203.

ZHANG, X. & BASARAN, O. A. 1996 Dynamics of drop formation from a capillary in the presence of an electric field. *J. Fluid Mech.* **326**, 239–263.